MF2059
Mechatronics Advanced Course

4D Printing with Closed-Loop Control

Final Project Report

Authors:
Anton Agerberg
Deyuan Chen
Jacob Edström
Jacob Häggqvist
Sresht Iyer
Linda Truong
Xiran Zhang

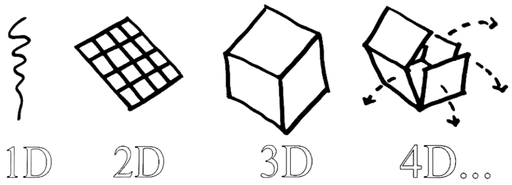

Abstract

4D printing can be seen as a natural extension to additive manufacturing, where the printed material can change shape over time. This is enabled through the introduction of smart materials, with self-induced actuation when stimulated by for instance voltage, heat, humidity or light. The 4D printing field shares the same advantages as 3D printing, enabling rapid prototyping through its inexpensive and facile embodiment of digital 3D models. However, it removes the limitation to static prototypes, allowing printed objects to move.

The potential applications come from a field as wide as for 3D printing. One highlighted application is furniture production, possibly eliminating the need for assembly and increasing the efficiency or transportation by an initially flat product. Other applications include self-healing materials and artificial muscles.

The novelty of the project is to introduce a closed-loop control to 4D printed materials. Previously open-loop controlled systems are sensitive to material variances and the external environment, whereas closed-loop control can enable the use of cheaper materials and enable the process in varying conditions. The increased robustness is realized through angular sensing with computer vision, current control and thermal modelling.

The project investigates two materials selected from an initial literature study of the field, namely Shape Memory Polymers (SMP) and a novel graphene-based Electro-Active Polymer (EAP) called Bucky Gel. Demonstrating their respective strengths, the two materials are combined for a concept design of an arm with a waving hand.

The Bucky Gel actuator is manufactured during the project with the assistance of a Chemistry PhD and a Mechatronics PhD, however to limited success. One successful bending attempt is achieved, but the manufacturing process was insufficiently described by previous researchers, resulting in a very low repeatability.

For the SMP, a repeatable manufacturing process is properly developed, reducing prototype variance. Despite this, the material shows a very non-uniform actuation, limiting its modelling capabilities. Instead, a model predictive control is developed, based on the angular velocity from experimental tests. This is successfully tested to accurately predict and control the final bending angle in some cases, while the system speed seems to limit it in other cases.

Acknowledgements

We would like to thank our stakeholder Lei Feng and our supervisor Binbin Lian for the support during this process and for enabling this exciting project. We also want to thank Qinglei Ji, Mechatronics PhD at both the Department of Machine Design and the Department of Production Engineering at KTH, and Tiziana Fuoco, Chemistry PhD at the Department of Fibre and Polymer Technology at KTH, for assistance with the Bucky Gel manufacturing process.

Contents

List of Figures

List of Tables

Nomenclature

BGA	Bucky Gel Actuator
CNC	Computer Numerical Control
CNT	Carbon Nanotubes
CV	Computer Vision
DC	Direct Current
DE	Dielectric Elastomer
DPI	Dots Per Inch
EAP	Electro-Active Polymer
FDM	Fused Deposition Modeling
I2C	Serial Communication Protocol
IPMC	Ionic Polymer-Metal Composites
MPC	Model Predictive Control
MSMA	Magnetic Shape Memory Alloys
PCB	Printed Circuit Board
PCV	Polyvinyl Cloride
PO	Polyolefin
PS	Polystyrene
PSPS	Pre-Strecthed Polystyrene
PWM	Pulse Width Modulation
RPi	Raspberry Pi
SCL	Serial Clock
SDA	Serial Data
SLM	Selective Laser Melting
SMA	Shape Memory Alloys
SMM	Shape Memory Materials
SMP	Shape Memory Polymer
SWCNT	Single-Walled Carbon Nanotubes

1 Introduction

1.1 Background

With the introduction of smart materials, their responses to external stimuli have been utilized for shape recovery, sensors, and actuators[25] [7] [8] [26]. In addition, attempts to combine smart materials and 3D printing resulted in 3D objects that are activated by environment and/or external stimuli. These stimuli-responsive additive manufactured objects were dubbed “4D printed”, first mentioned 2013, highlighting time as the fourth dimension[23]. Shape morphing after printing is the main characteristic of 4D printing. Shape variations in 4D printed objects can be induced by different external stimuli, to cause expansion, shrinkage, or folding of the printed objects. For example, self-folding and automatic response of 4D printed objects was obtained using smart materials. Three main important aspects of 4D printing include Stimuli, Material and Printing Technology. Simulation software is also a major part of 4D printing, and it encompasses all the above-mentioned aspects.

4D printing has advantages that cannot be found by simple 3D printing. By printing objects as 2D sheets, it saves a lot of space and provides a much more efficient means of transport. With the help of 4D printing, it is possible to build actuators that work without wires, motors or batteries. This makes them very desirable for the research of smart devices and nano actuators. [21]

Some potential applications are for instance furniture, self-healing materials and artificial muscles, all benefiting from self-induced actuation. Other potential applications are also shown in the radial diagram in figure 1. Just as 3D printing has the potential to revolutionize many industries, 4D printing can make all of that move.

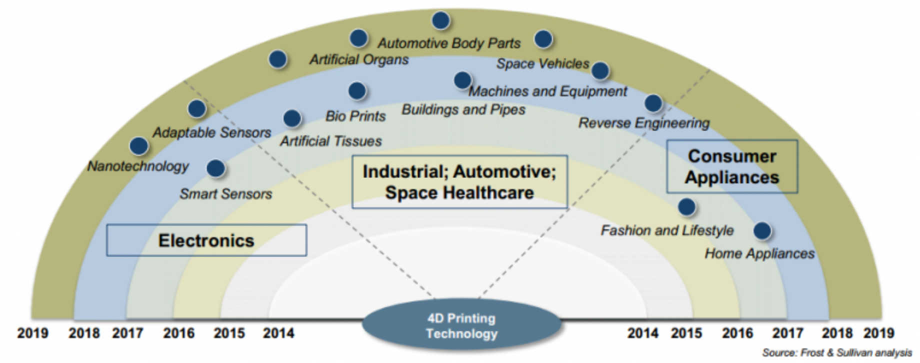

Source: Frost & Sullivan analysis

Figure 1: 4D Printing applications

However, 4D printing is at a very early stage, as can be seen in the Gartner Hype Cycle of 2018, shown in figure 2. There it can be seen that 4D printing is far behind for instance Quantum Computing, which means there has not been much research done in 4D printing yet. This means that there are not a lot of materials with these properties to be directly printed. Research in the area will therefore have to be jointly done from a Mechatronics control perspective, stating the requirements needed to fulfill application ready 4D printing, in parallel with materials science to enable these new materials.

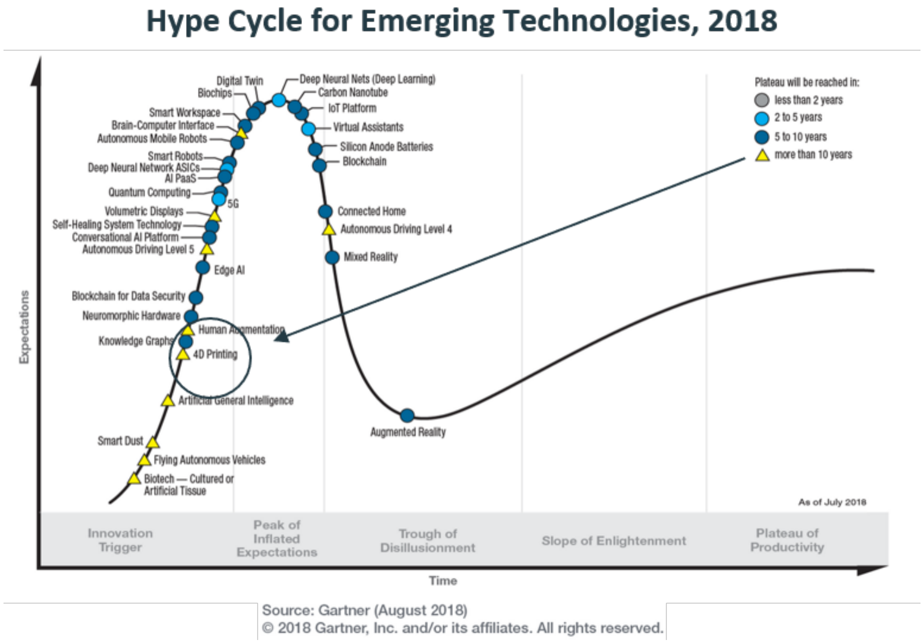

Source: Gartner (August 2018)
© 2018 Gartner, Inc. and/or its affiliates. All rights reserved.

Figure 2: Gartner Hype Cycle 2018

1.2 Project Description

This project has been issued by the Mechatronics Department of the Royal Institute of Technology (KTH), with the aim of enabling further research in the field of 4D printing with closed loop control. The project is thus open-ended, with the goal to produce a prototype by 4D printing, with the ability to change shape, self-assemble or otherwise respond to stimuli that can be controlled.

The proposed closed-loop control has several potential advantages. As the topic concerns material deformation through stimuli, the external environment may have a significant impact on the process. Open-loop controlled 4D printed objects will therefore behave differently depending on location and time, or alternatively be limited to very fixed conditions. Closed-loop control will therefore enable a more realistic use of 4D printing, enabling a similar system performance in varying conditions. An additional advantage is that closed-loop control will enable a similar performance with materials with lower tolerances, as varying material properties between batches can be compensated for, enabling the use of less expensive materials. The project will therefore attempt to realize the closed-loop control with at least one material with this cost-effective character.

As a preparatory step, there was a need for a literature study on different "smart materials" that has the mentioned response to stimuli. The literature study was to be carried out with two additional requests in mind, namely embedded electronics and closed-loop feedback control, aligning this project to the Mechatronics division. The embedded electronics mostly focus on printable sensors, which enables the feedback control. The closed-loop feedback control for 4D printed objects is a novelty which has not yet been researched, which gives this project a highly experimental character.

1.3 Requirements

Requirements for this project have been jointly established by the project team and the stakeholders. One requirement concerns the definition of 4D printing, that the created prototype conceptually has to be able to be built by a multi-material printer. This requires a flat, layer-by-layer structure, but can at this stage be fabricated through other means than additive manufacturing. The second requirement is that closed-loop control should be made possible through the project design, with controllable actuation systems and adequate sensors with limited system impact.

1.4 Delimitations

The main topic of this project is the introduction of a closed-loop control for the 4D printed material. The scope will be limited to the investigation of the impact this has to chosen systems and also to investigate the differences between closed and open loop control of the system.

At this very early stage of 4D printing, materials science can be considered a hot topic. It is clear that much can be done in the scope of developing new materials that can have these useful properties. Although, as this is a project done by the Mechatronics division, the scope was restricted to only existing materials. However, they were allowed to have an experimental character, due to the lack of existing materials with desired properties.

A clear delimitation for the project is that nothing will be printed, as no general advanced multimaterial printer exists today. To not limit the research to only existing printers, the project is instead limited to a prototyping stage, developing a method with selected materials which later conceptually could be printed.

The project will be carried out over 15 weeks, which poses a clear limitation to the research scope of the project. The project will focus on creating a repeatable foundation for tests with the chosen materials, in the cases where it is possible. For tests with more experimental materials, the chemistry process of manufacturing the material will put restraints on the scope and quantity of tests.

1.5 Report Disposition

The report is structured in the following manner.

Following the *Introduction* comes a *State of the Art* review of the 4D printing field, serving as a theoretical background to the project. The project direction is based on the findings in this section, identifying materials and manufacturing processes best suited for the proposed closed-loop control.

Next comes a *Project Design* section, stating the project specifications and requirements, mentioning which materials and equipment that has been selected.

The section *Methods & Implementation* covers the implementation of the specified systems from project design, describing the task specific engineering methods to realize the system.

Verification & Validation explains how the subsystems were verified with unit tests and how the complete system performance was tested and validated to the stakeholder requirements.

In the *Results* section, all project results are presented. This covers both the SMP tests as well as the Bucky Gel manufacturing process, which by itself is a result of the project.

The results are discussed in the *Discussion & Conclusion* section, summarizing notable project results.

Future Work looks ahead and specifies what needs to be targeted next by further research in the field.

2 State of the Art

2.1 Materials

In this section, the active/smart materials of 4D printing are explored. In the context of 4D printing, the term smart materials is commonly used, meaning materials that have the ability to change their shape or properties via external stimuli. A summary of these materials can be found in Table 1. Smart materials can be dichotomized between Shape Memory Materials (SMMs) and Non-Shape Memory Materials [11]. The choice of material for 4D printed objects depends on which stimulus-response that is desired.

Shape Memory Materials
The key property of SMMs is that the materials can return to their original permanent state from a deformed temporary state, or conversely, transform from an original state to a permanent and final state, via an external stimulus. The SMMs can be categorized into two categories: Shape Memory Alloys (SMAs) and Shape Memory Polymers (SMPs).

SMA materials change shape when a temperature stimulus is applied. This phenomenon is called the Shape Memory Effect (SME). SME is a result of the transformation between two different crystalline phases in the SMA. However, thermal memory is not the only property, the material also has mechanical memory due to its superelasticity. This means that the alloy can recover a lot of the strain after and before the shape transformation. A commonly used SMA material in engineering applications is NiTi (nickel-titanium) [11].

Magnetic Shape Memory Alloys (MSMAs) are a subset category of SMAs, which produce forces and deformations in response to a magnetic field. The thermal shape memory effect has been obtained in these materials as well. Typically, MSMAs are alloys of Nickel, Manganese and Gallium(Ni-Mn-Ga). The process of 4D printing utilizing MSMAs is in its infancy; some investigations have been conducted concerning the additive manufacturing route of producing functional net shaped parts from pre-alloyed magnetic shape memory Ni-Nn-Ga powders[16].

SMPs respond to different stimuli such as temperature, light, moisture and magnetic fields [11]. One area of investigation is SMP composites with glassy fibres, where the fiber architecture is controlled (amount, location and orientation of the fibres) to decide in advance the reaction of the active material. The SMP fibres are sandwiched between an elastomeric matrix [17].

There exists a proof-of-concept 3D printed lamp made by Harvard University researchers, where Prestretched Polystyrene (PSPS) is used as the active SMP material, with thermal energy as stimulus. The active material is squeezed between layers of copper circuit, paper and foam. When heat is applied, the original flat shape of the lamp is transformed into the lamp shape found in figure 3 [20].

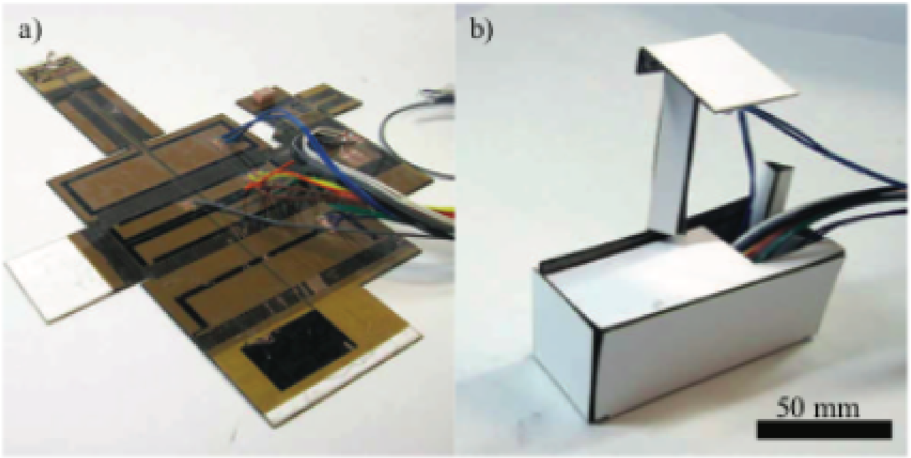

Figure 3: Proof-of-concept lamp: a) Original shape. b) When heat is applied. [20]

Additionally, multiple SMP materials are documented in Felton's research report. E.g. a material called polyolefin (PO) that shrinks uniaxially, and another material called Polystyrene (PS), that shrinks biaxially [5].

Polyvinyl chloride (PVC) is also a SMP material that responds to thermal energy by contraction and folding of the edges. PVC is used in the proof-of-concept "bakeable robot" made by MIT researchers [3].

Comparing SMPs and SMAs, the SMPs have the advantages of lower density, lower cost, higher strain recovery, good controllability over the recovery temperature and the simplicity of programming shapes. It is also possible to modify SMPs chemically to achieve biocompatibility and biodegradability. The main drawbacks of the SMPs are that they have comparatively low modulus, low strength and low operating temperatures [11].

Non-Shape Memory Materials
Hydrophilic polymer absorbs water and forms a hydrogel that can expand to approximately 150-200% of its original volume. When the 4D printed object is placed in water, the active material of the object absorbs it, swelling to form the rigid material and bending to a desired structure [23]. The main

disadvantage of this material is that it gives rise to mass diffusion, limiting response speed. Moreover, this material exhibits low controllability as it only can shift between two binary state structures, limiting its programmability and usefulness [24].

Piezoelectric material responds to mechanical stress as stimulus. When stress is applied, the material produces electrical charge or voltage. Piezoelectric polymeric materials are suitable for systems with requirements on mechanical flexibility, biocompatibility, small active elements and solution-based processability. However, fabricating this material into complex structures or small active elements is still fraught with difficulties, calling for improvements in manufacturing procedures. However, a piezoelectric material that has been manufactured and utilized with some success is a combination of barium titanate ($BaTiO_3$, BTO) and a polyethylene glycol diacrylate (PEGDA) matrix [11].

The somewhat novel electroactive polymers (EAPs), are flexible and functional materials that can produce significant changes in either size or shape under electrical field excitation. EAPs are considered strong alternatives to conventional actuators and sensor materials for numerous reason. E.g. due to their small electrical energy consumption, light weight, compliant properties, biocompatibility, ability to operate in air and aquatic media, insensitivity to magnetic fields and simple fabrication processes. Ionic polymer-metal composites (IPMC), Bucky Gel and dielectric elastomers are all EAP materials, constituting a branch of intelligent materials [1].

More specifically, IPMCs are synthetic composite nanomaterials that display artificial muscle behavior under an applied voltage or electric field. A typical IPMC consists of a polyelectrolyte membrane plated on both faces by a noble metal. Transport of hydrated cations within an IPMC beam under the applied voltage and associated electrostatic interactions leads to bending of an IPMC beam. IPMCs have light weight and can undergo large bending deformations under the influence of low driving voltages. They operate best in a humid environment [1].

Bucky Gel is one of the most recently developed ionic EAP intelligent materials. A Bucky Gel actuator consists of three layers. An electrolyte layer constitutes the middle layer, consisting of a polymer and ionic liquid. This middle layer is sandwiched between two layers of electrode materials consisting of single-walled carbon nanotubes, polymers and ionic liquid. When a voltage is applied over the Bucky Gel actuator, cation and anion of the ionic liquid move to the electrodes, causing the actuator to bend. The direction of deformation depends on the polarity of the voltage. Conversely, Bucky Gel can also can be used as a sensor when external actuation is applied, as the displacement induces a voltage over the electrodes [9].

Dielectric elastomer (DE) actuators are constructed utilizing a similar sandwich structure as the aforementioned Bucky Gel actuator. The DE actuator is essentially a dielectric elastic membrane material with its surfaces coated with a flexible electrode layer. When a voltage is applied, the top and bottom surfaces of the DE actuator accumulate polarizing charges. The active and negative charges attract each other producing a static Coulomb force. This force reduces the thickness, and consequently, expands the surface area of the material [19].

Pneumatic actuators are yet another option for non-shape memory materials. Pneumatic pouch motors that contract when they are inflated has been used previously for actuation in self-folding robots [22, 18]. By attaching these actuators over hinges, it is possible to produce a controllable system with a high resolution, capable of actuating smoothly back and forth within its operating range. The pouch motors are made from two thin plastic sheets that are molded together. Due to the thin geometric shape of pouch motors, they are easily integrated in a flat design. The manufacturing process is compatible with mass production, albeit with some unnecessary complexity as a complete product currently requires separate production and attachment of the actuators. In other words, there is currently no 3D printer on the market that is able to create these pouches as part of a rigid structure. However, that does not mean that it violates the scope of 4D printing. It can be argued that these limitations are technical and not conceptual.

Categories	**Materials**	**Stimuli**	**Properties**
SMAs	Ni-Ti	Temperature	High recovery strain
Magnetic SMAs	Ni-Nn-Ga	Magnetic fields	High recovery strain
SMPs	PO, PS, PVC	Temperature, light	Low cost, high recovery strain
Hydrophilic polymers	Hydrogel	Moisture	High expanding features
Piezoelectric	$BaTiO_3$, BTO, PEGDA	Voltage	Reversible i/o features
Electroactive polymers	Bucky Gel, IPMC, DE	Voltage	Biocompatibility, low energy consumption

Table 1: Summary of smart materials

2.2 Manufacturing

3D printing is already well known as an established and effective additive manufacturing process. 4D printing is an exciting new take on additive manufacturing, sharing many similarities and building upon the concepts of

3D printing, but doing so using 'smart materials' that can actuate under certain stimuli.

This type of process is made possible through recent technological advancements. For example, the PolyJet Printing Technology developed by Stratasys Connex recently made great progress in the handling of multiple material printing. Similarly, Selective Laser Melting technology, the process of using a high energy density laser to melt metal powder in order to build a well-distributed 3D structure without any adhesive or other mechanical support, was recently realized. These two examples, and numerous other technological advances, are what drives the development of 4D printing forward.

Polyjet Technology for Multi-Material Printing

Normally, additive manufacturing technology aims to shape different materials in a pre-calculated distribution throughout one printing process. Different properties of materials such as swelling ratio and coefficient of thermal expansion make it possible for the structure to form according to a predetermined design. Naturally, the choice of printing technology is done in accordance to what kind of material is to be used.

4D printed objects need to incorporate both active materials (to actuate deformation) and inactive materials (to provide structure) in order to deform in a predictable way (and thus have any useful application). Because of this fact, multi-material solutions have to be used. In this regard, the Polyjet printing technology from Stratasys Connex, illustrated in figure 4, is an excellent and interesting development. PolyJet is a powerful 3D printing technology that produces smooth, accurate parts, prototypes and tooling. Materials are jetted as a liquid and once a layer of material is deposited, it is cured immediately by UV light to form into a solid. Since jetting different materials from different nozzles is possible, composite materials with various properties could potentially be printed in single cycle, making this technology ideal for 4D printing applications. However, a major limiting factor for this technology is that it can only be used for UV-active photopolymers, which are not durable over time.

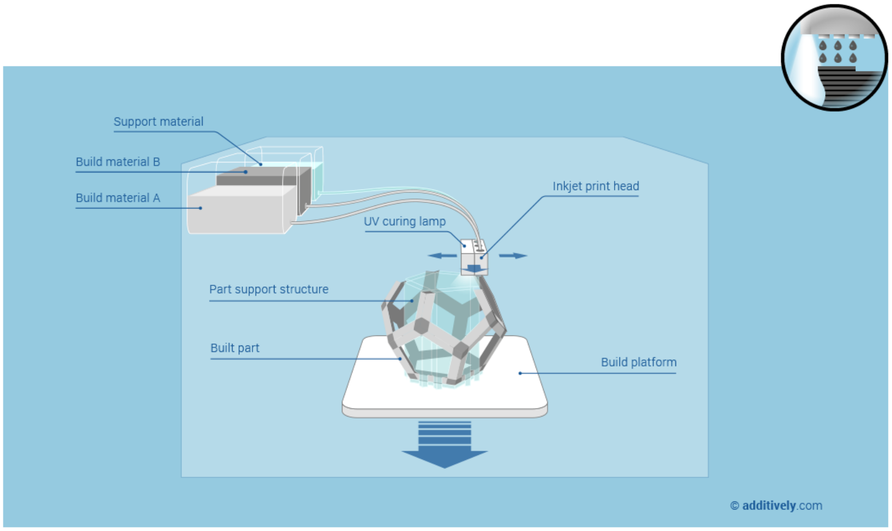

Figure 4: Photopolymer Jetting technology.

As an example, hydrophilic UV curable polymer could be printed through Polyjet printing technology. When the polymer is exposed to water, the structure absorbs it and creates a hydrogel, expanding up to 150 % of its original volume [2]. Presently, the printer Connex3 Objet500 is able to mix three different resins in precise ratios within a single print operation, and with a range of 45 possible colours [7].

Selective Laser Melting (SLM) technology for SMAs
The second possible choice of printing technology is Selective Laser Melting (SLM) technology for Shape Memory Alloys (SMAs). The process of selective laser melting is as follows. The machine distributes a layer of metal powder onto a build platform, which is then melted by one laser or multiple lasers. A scanning mirror is put above the platform to selectively refract the laser, selectively melting the metal powder. After a layer is completed, the build platform will be lowered and the cycle begins anew with the next layer. This technology is very promising in regards to 4D Printing implementations, specifically for SMAs.

The main advantage of this method is that parts could be manufactured in standard metals with high density (above 99) and good mechanical properties. However, the technology is expensive and the process is rather slow. Tolerances are also limited (though this could be improved through post-processing).

Fabrication technology for SMPs
There is some potential flexibility in fabrication methods for SMPs. Planar fabrication techniques such as laser cutting and lithography are more quick and inexpensive in producing SMPs of certain geometries when compared to additive manufacturing. An example of this is found in the methods used by [5]. The basic idea of the method is utilizing composites of SMP bonded to paper, stimulated by joule heating via resistive circuits. The composite can be assembled at a low cost by laser-cutting each layer separately, then bonding them together with silicone tape and/or alignment with pins.

The composite used consists of a layer of 510 μm paper substrate (Cold Press Bright, Epson), two layers of 18 μm copper circuits on 25 m polyimide (AC181200R, DuPont), and a layer of prestretched polystyrene (PSPS) (Grafix Inkjet Printable Shrink Film, Grafix). The circuit patterns are printed onto the copper-clad polyimide using a solid-ink printer. The ferric chloride etch tank is subsequently used to etch the circuits by removing the excess copper. The PSPS and the paper layer are cut into shape using a C02 laser cutter (VersaLaser 2.0, Universal Laser Systems). The final step is aligning those layers in a specific order with pins and bonding together with 50 μm double-sided silicone tape (ARclad 7876, Adhesives Research).

This method is quick and inexpensive when considering the equipment and time limit. According to Felton's article, even the more complicated designs only took approximately one hour to assemble by hand, utilizing only a laser cutter, a solid ink printer, and a ferric chloride etching tank[5].

2.3 Further research on closed-loop 4D printing

Feedback
In this early stage of 4D printing technology, the research so far has been focused primarily on printing actuation mechanisms, which of course is a central area of this new field, given that the goal is to print materials that can change shape in response to stimuli. Key aspects such as materials, manufacturing and geometry have been investigated, to perfect the motion of the 4D printed detail. However, as a result of this focus, discrepancies between calculation and experimental outcome has almost always been dismissed as modelling errors or inaccuracies in the folding process, rather that problematized and analyzed in pursuit of an alternative solution [6].

Overall, the 4D printed process has been regarded as an open loop system, without any feedback control. This will inevitably limit the performance of the system for a number of different reasons. Firstly, any model procured for these materials will have some kind of model error, however small. Secondly, when the conditions (internal & external) of the model vary or no longer apply, the validity of the model may decrease drastically. For instance, this could be caused by varying temperature, humidity, electric and magnetic fields emitted by nearby devices, differences in luminance, load disturbances and vibrations. This will serve to severely limit applications in areas with strict tolerances, such as production tools and robotics, as well in areas with high precision requirements, such as medical applications.

The proposed addition to this research is to introduce a closed-loop feedback system, which can ensure a high precision in actuation. Thus, controllability has been investigated as an extra property for the presented materials in this report. To enable a closed-loop system, there is a need for an actuation mechanism with high resolution, in order to apply stimuli appropriately.

Additionally, a sensor or monitoring device is needed in order to track the actuation with high precision. Either with an external sensor, or an embedded sensor.

One example of an external sensor is a high precision camera or laser detector that can measure the output of the 4D printed device. The advantage of this method is that it does not affect the system itself or change its dynamics.However, the drawback is that it may not be as mobile as the device itself, and will need to follow it. If the position of the object changes, i.e. it moves or rotates, this method may have a reduced precision and may lead to more complex design to maintain accuracy. To enable depth perception, more than one camera is needed, and thus the use of this may be limited to enclosed spaces.

The other option is an embedded sensor, which is attached to the 4D printed device itself. The advantage of this is that the sensing may be angle-independent and less affected by motion, in the sense that nothing will need to follow the device. However, motion may also introduce other disturbances to the sensor, which will have to be accounted for. Additionally, the properties of the system itself will be changed with the introduction of an embedded sensor.

Here there may be two options, of either printing the sensor within the device itself or attaching it at a later stage. Printing the sensor may limit the manufacturing to printing techniques that enable built in sensors, while also enabling measurements which otherwise can be hard to capture. In order to minimize this limitation, there have been studies on alternative filler materials for regular 3D printers, such as ”carbomorph” [12]. Without the need to alter the printer, string sensors can be printed and measure deformation through flexing. More sophisticated machines are also being developed, stretching the definition of 3D printing by merging multiple machines, basically forming a “swiss knife” of manufacturing technologies. One example is the multi3D printer [2], incorporating FDM printing, CNC micromachining system and conductive ink deposition systems to enable printable electronics. The study also proposes embedding copper wire conductors into FDM-fabricated substrates, to increase the durability for use in more extreme environments. There is a significant disadvantage in terms of replaceability of electronics with the printed method, but also a robustness in terms of reduced external stress.

The main disadvantage of the embedded sensors is its limited accuracy. Therefore, a combined approach could be used, using the high precision camera to calibrate the embedded sensor. This calibration can be done without unnecessary motion, where the camera has its highest accuracy, and the embedded sensor can be used from there on, not limiting the applications of 4D printed devices with embedded sensors.

Controllability

Among the materials studied, it has been hard to find those with a controllable output. For a feedback system to work, there is a need to control the actuation with a high resolution, and be able to have some kind of proportional relationship between input stimulus and output folding angle.

The shape memory materials have a predetermined angle, based on the geometry of the hinge. It bends once its activation energy has been reached, through a threshold temperature value. Piezoelectric materials have the proportional property, but the output force is very weak and most suitable for sensors. One option is to study the bending process of the shape memory material, and model its behavior. Then, it might be able to stop the bending process half-way through, as the folding is rather slow, where it could be seen as a dynamic process rather than two discrete states. The benefit of this method is that the printing complexity is reduced, as it only requires one active material in a construction that also has basic structures without a need of controllability. However, once actuated to a certain angle, the material will first have to be reset to its initial state to achieve a smaller angle, thus not operating smoothly back and forth within its operating range.

One other option is to include the pneumatic actuators. While this option provides a controllable system, it can't be printed, and is thus less optimal for this purpose. The materials needed are neither expensive nor hard to acquire, but there is a need for the melting equipment that forms the pouches, which require CNC milled metal forms.

Most promising of the options is the Bucky Gel material, which has a voltage controlled output. Not many applications have used this material yet, so it is more experimental. Although, it has the benefit that it can be printed with traditional methods, which would fit the scope of this project best.

3 Project Design

This section cover the selected design, components and control solution.

3.1 Concept Design

The project was decided to be focused on researching two of the materials found in the State of the Art study, namely the heat controlled Shape Memory Polymer (SMP) and the voltage controlled Bucky Gel. The materials were to be compared and possibly combined, demonstrating their respective strengths. Both actuators enabled a flat, layer-by-layer design, identified as suitable for a future 4D printing process.

The selected design was an origami-based prototype with a controllable folding process, in the shape of a humanoid arm seen in figure 5. The SMP would be used for the "heavy-lifting" of the shoulder and elbow joint in a double hinge design, demonstrating its relative strength and permanent deformation, while the Bucky Gel would be used for a continuously waving hand, demonstrating its continuous motion control. Ideally, the Bucky Gel would also be able to be used as an angle sensor, for the closed-loop feedback control.

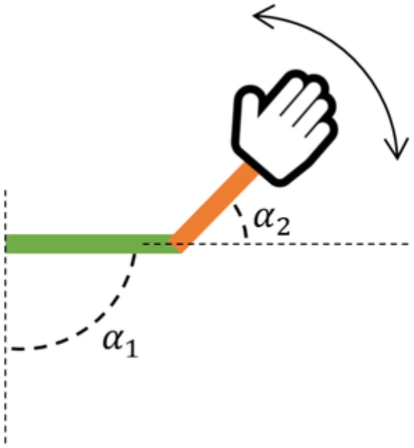

Figure 5: Concept Design

For this system to be realized, there was a need for heating control for the SMP. This was realized with a custom made flexible heating circuit, driven by a closed-loop custom made current driver with current sensing. To model the system for the heat stimulated SMP, a thermal sensor was used. Even though Bucky Gel could be used for angular sensing, this would have to be calibrated to an external system, which is why computer vision was selected instead as the main approach for this.

3.2 Materials

3.2.1 Bucky Gel

The Bucky Gel actuator is a novel electro-active polymer(EAP), which can directly transform electrical energy into mechanical work. It was therefore selected to be used for the project, as this low-voltage stimulation shows high potential for controllability. However, Bucky Gel has not been widely used in 4D printing, one of the reasons is the lack of memory effect. The voltage has to be applied constantly to keep the Bucky Gel shape unchanged after the desired deformation process.

In tests made by Norihiro [9], a strip of the Bucky Gel actuator was fixed in a cantilever and an input voltage of ±2 V with a frequency of 0.2 Hz was applied. The displacement at a point near the tip was measured by a laser displacement meter. The Bucky Gel film bent smoothly in response to low applied voltages, in the direction of the positive pole side.

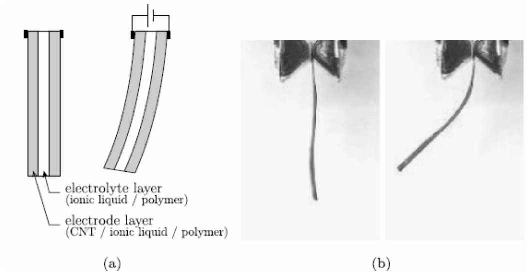

Figure 6: Bending motion of a Bucky Gel actuator: (a) Schematic diagram. (b) Bending response.[9]

It can be seen from the figure 7 that the displacement of the Bucky Gel followed the input voltage with a quick reaction speed. It has with other words previously been proved to have a high-resolution, repeatable and predictable movement, although actuated in an open-loop system in a single test environment. The project aimed to build on this first material verification and enable closed-loop control for a more robust system performance.

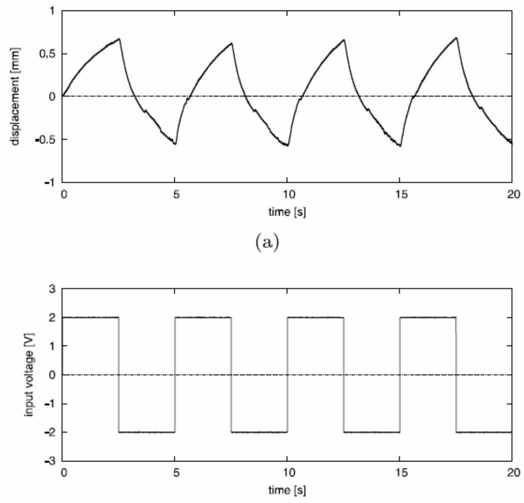

Figure 7: Bending response of a Bucky Gel actuator: (a) Displacement. (b) Input voltage.[9]

Bucky Gel could not be directly bought, and had to be manufactured by the project team with the assistance of both a chemistry PhD and a mechatronics PhD. The layered structure sandwich an electrolyte layer between to electrode layers, the latter made of single-walled carbon nanotubes. This nanomaterial is made from single-atom layers of graphene, rolled to a cylindrical shape. As such, the project also investigates the potential of graphene-based actuators.

3.2.2 Shape Memory Polymers

Shape memory polymers were identified as the other interesting material, more in line with the intention to test a cheaper material with higher variance. The described advantages of closed-loop control was certainly put to test with this material, with a more complex actuation through heating. However, as this heating still was voltage-controlled, a proper mechatronics control system could be built around it.

The strategy was to mimic Felton's application using SMPs [5]. This self-folding method is inexpensive, sequential and localized. The used material is composites of SMPs bonded to paper with temperature as stimulus. The heating is achieved by a resistive heating circuit, integrated in the design. The SMPs utilized in Felton's article were polyolefin (PO) that shrinks uniaxially and polystyrene (PS) that shrinks biaxially, where both SMPs can contract to 50% when heated above its transition temperature (Tg = 95 °C). The PO is used when doing the experiments and PS is used when building the structures shown in figure 8 [5]. The experiments have been made with applied current of approximately 1.5-2 A, during 1-2 minutes. For the pyramid structure, the resistive circuits were connected in series (folding all hinges at the same time) while the self-locking slot-and-tab used sequential folding [5].

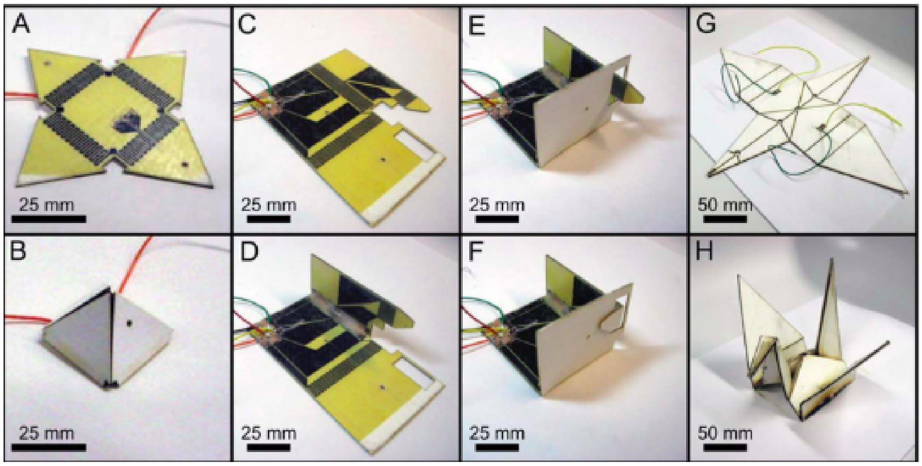

Figure 8: Demonstration of Felton's three self-folding structures.[5]

In the experiments made in Felton's article, the folding angle was measured as a function of time with a fixed current. The result showed that if the current or the trace width were decreased the folding angle would also decrease. It is believed that the reason is because of the geometry during folding. As seen in figure 9F [5], when the SMP begins to bend it detaches from the resistive circuit and therefore the heat flux in the SMP reduces. When the SMP temperature drops below the transition temperature, it solidifies and the folding stops.

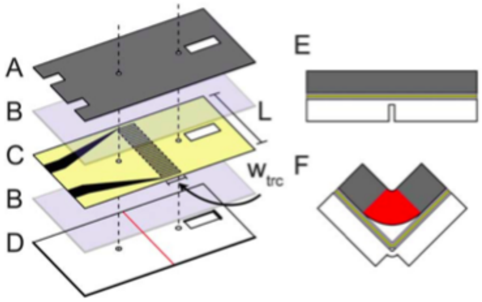

Figure 9: The self-folding composite samples used in Felton's characterization experiments. A - SMPs. B - silicone tape. C - resistive circuit copper trace on polyimide sheet. [5]

For this project, two different shape memory polymers have been investigated, both of the pre-stretched polystyrene type. Following Felton's article, Graphics Ink-Jet Printable Shrink Film was used, but only found in an edition with a shrinkage to 20% of the original shape. To compare with a more similar performance to the article, Shrink Me Shrink Film was also used, with a shrinkage to 40%. The shape memory effect is found in the shrunken form, to which it returns when heated up in its pre-stretched form.

3.2.3 Support Materials

Paper Structure
The main structure will have to be built by a stiff but still light material. For repeated tests, parts of the design had to levitate in the air without support, even with perforations in the material, without reclining by the gravity. At the same time, it had to be light enough to be lifted by the shrink film. Based on these parameters, Epson Cold Bright Press paper was chosen, which filled all requirements and was cost effective in the context.

Adhesive
To join the layered design, double adhesive tape was used. As the heating element would heat up to temperatures around 200° C, a heat resistive Kapton Polyimid tape was used. It was rated to withstand 300 ° C for one hour and 260 ° C for longer periods, which was well suited for the project. The thickness was also of interest, and this tape is only 0.1 mm thick, which makes the design slim and suitable for printing.

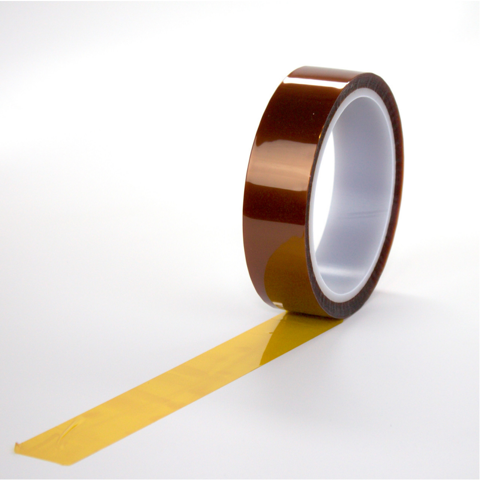

Figure 10: Heat resistant kapton double adhesive tape

Heating circuit

The heating circuit was made with a flexible copper laminate, a Dupont Pyralux AC 181200R. The product name stands for an 18 μm thick single sided copper layer on a 12 μm polyimid sheet. For research with foldable structures, the flexibility of the material was important. The thickness also played an important role, determining the resistance of the copper traces for fix trace widths from limitations in the following manufacturing process.

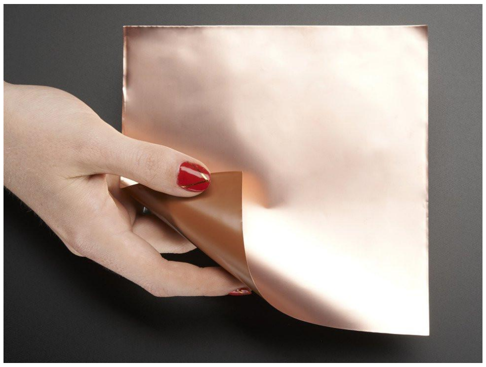

Figure 11: Dupont Pyralux flexible copper laminate

3.3 Sensors

3.3.1 Computer Vision

Since the novelty of 4D materials is the capability to deform over time when subjected to external stimuli, one needs a method of measuring that deformation reliably in order to model and eventually control said deformation. For this purpose, a Computer Vision-based algorithm was to be developed. The main advantages of this approach includes an absence of impact on the system when measuring deformation angle, in contrast to other potential solutions, such as flex sensors or potentiometers. Unlike many other methods, its output also does not need to be tuned and only requires a single external module for image capture, in this case a Logitech C920 Web Camera; the rest is taken care of on-board the RPi. This solution also offers better scalability than mechanical sensors, since capturing additional angles and shapes amounts to simply changing the code governing the algorithm. Having the sensor external to the prototype does however make it sensitive to variations in placement. Luckily, this can be easily worked around by fixed camera placement in the prototype environment. The performance requirements for the implementation of the Computer Vision solution are represented in table 2.

Performance Metric	**Requirement**
Sample Time	$< 0.4s$
Noise	$< \pm 1$ degrees
Reliability	> 95 %

Table 2: Computer Vision Performance Requirements

'Noise' is defined as the maximum variation around a fixed measurement and 'Reliability' is the percentage of samples where valid measurements were registered (i.e. the correct bodies were detected and properly sorted and identified). Additionally, the implementation needs to support not only single hinge designs similar to the one seen in figure 12, but also double hinge designs of the type described under concept design.

It was decided that a solution where hinges are marked in three locations as seen in figure 12 was to be used. For the corresponding double hinge design, an additional marker was simply added to its endpoint, resulting in four markers (one on each hinge corner, one in each endpoint). Besides serving to allow for a simpler implementation of the algorithm, there were also a number of other practical advantages to this.

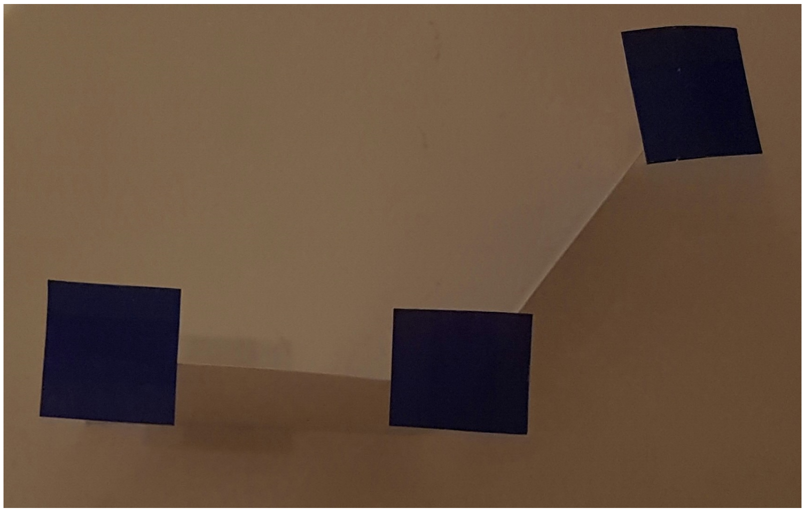

Figure 12: Computer Vision Markers

Performing image processing on the SMP-hinges in their entirety, while certainly very possible, would introduce numerous unnecessary problems that would need to be accounted for in the script, such as the SMP deforming unpredictably along the inside of the hinge, likely making the edge-detection function pick up new contours, potentially introducing unpredictable variance in the angle readings. Such an occurrence would not only be an obstacle to the eventual implementation of feedback control, but also produce lower quality data for the modelling and control part of the project.

Since the requirements placed on the Computer Vision solution emphasized accuracy and reliability over flexibility and superfluous complexity, the decision to stick with the marker-based solution was uncontroversial.

3.3.2 Thermal Sensor

As the SMP is heat stimulated, temperature measurements may be very useful for the modelling of the system. Temperature measurement in this setup is performed with the help of the MLX90621 thermal sensor. It is an i2c device and hence uses the i2c protocol to measure temperature values and send them to a microcontroller. This sensor can measure temperatures in the range of -20 to 300 degree Celsius, along with an operating temperature of -40 to 85 degree Celsius. It requires a 2.6 v supply and can measure the ambient temperature as well as the IR radiation from the objects in its field of view (60 degrees x 16 degrees) to measure the temperature and display them in an array of 16 x 4 values.

The wide field of view of the sensor and the multiple pixel values makes the sensor placement less critical, as the highest temperature measurement can be extracted. This is suitable for consistency between different test setups, eliminating sensor inaccuracies due to misalignment, in favor of the research focus of the project. This is valued higher than sensor efficiency, which otherwise could be achieved by a single-valued sensor like the MLX90614. For this sensor, there will only be $18 + 18 = 36$ bits at the most. This makes this device faster to access and does not require a microcontroller to access a lot of addresses in order to read the temperature. This single value is the average of the temperature values inside its cone field of view, which for that sensor is 90 degrees. This requires the sensor to be put very close to the design, in order to not distort the temperature reading by averaging a field outside of the heated area. By design, it will therefore not be able to capture the entire heating area, and to not exclude potential valuable information for the modelling of the system, this single-valued sensor is not chosen.

3.3.3 Current Sensor

For a closed-loop current control to work, there is a need to monitor the current, done by a current sensor.
The INA219 is a current shunt and power monitor which uses the i2c interface. The device monitors both shunt voltage drop and bus supply voltage. With a known shunt voltage value, current readout can be read.

The INA219 senses across shunts on buses that can vary from 0-26 V. The device uses single 3-5.5 V supply, drawing a max of 1 mA from the supply. This sensor can operate from -40 to 125 ° C and can measure currents up to the range of ± 3.2 A with a resolution of 0.8 mA. If the shunt resistor across the sensor is changed from 0.1 ohms to something lower, e.g. 0.01 ohms, then the range of the sensor can be as high as ±32 A with a resolution of 8 mA.

3.4 Control & Driver

3.4.1 Control System

For the controller hardware, the setup initially used the Beaglebone black to perform the image processing, and attempted to use the i2c buses on the Beaglebone to integrate all the sensors together. But given the lack of support for using the i2c protocol, and also the slow performance of the Beaglebone, it was decided to use the raspberry Pi instead, since the support for libraries needed for the i2c devices, as well as the performance with the image processing were both superior. Next, it was attempted to use the raspberry pi as a central server/node that connected the i2c sensors and the camera sensor together at one place while getting data from all of them. After several trial and error methods, it was found that the sheer volume of data flowing through the i2c buses was too much for the raspberry pi to handle, given that its i2c protocols were not made for this sort of data processing. But since the computer vision algorithm still needed a powerful processor, the Pi was still needed.

The solution to this was to use an Arduino, which could handle the i2c sensors, to link with the raspberry pi serially, so that the Arduino can read the values from the sensors and send them serially to the raspberry pi, which the pi can use while running the computer vision algorithm simultaneously.

The requirements for the system is to enable a sample time of 0.6 seconds, which is derived from Felton's article [5] of a similar process, but with an extra 0.1 seconds for a margin for controller execution.

3.4.2 Current Driver

In order to control the heat propagating on the SMP material from the copper circuit pattern, a design based on PWM signal control was suggested. By controlling the voltage, and subsequently the current, the temperature can be increased/decreased based on angle measurements.

As the current will need to be high for the heating circuit to work, it is important that the current driver can handle this. Therefore, the resistance of this design should be as low as possible, to reduce the burnt off power and produce as little heat as possible. As most motor drivers and current drivers are not rated for more than 2 A, this current driver was customized and manufactured by the team.

4 Methods & Implementation

This section covers the implementation process of the project design, covering the strategy to produce the components as well as control algorithms.

4.1 Project Management

4.1.1 Agile Project Management

Given the research focus of this project, it was executed in an agile form with Scrum methodology. Material properties were unknown and in some cases the material had never been successfully manufactured yet, which created obvious limitations to design choices. Thus, the team had to be flexible to align with the progress of the research, to switch roles when certain processes were put on hold for manufacturing delays. The novelty of the project also imposed a limitation that none of the team members had previous experience of the process nor the materials, which made no one the expert on a certain field. This way, the rotation and shifting involvement led all members to be more closely connected to the processes as well as introducing more ideas to solve these new problems.

The scrum methodology was therefore well motivated, with weekly meetings and a continuous re-prioritization of tasks. Each meeting started with a retrospective of current progress, what all team members had done according to last week's distributed tasks. Open discussions were held where everyone had the right and chance to influence the development of all tasks. Interest in the task was the main driver to whom the task was delegated, most times aligning it to the initial role division but enabling a flexibility therein. Clear objectives as to what was needed to be done before next meeting was always done at the end of each meeting, where everyone had the chance to confirm that they knew what to do next.

Slack was used as the project communications tool, which was agreed to be closely monitored by the team members to allow for this flexible arrangement. In this way, all team communication was always gathered in one platform, easily found at later times.

4.1.2 Iterative Alignment

Frequent meetings were held with the project stakeholders, to update on the progress of the research. This enabled the team to iteratively align the research focus to the interest of the stakeholders and to validate the system performance to the stakeholder requirements. This resulted in a continued focus on the Bucky Gel manufacturing process even though the process proved to be harder than expected, where following tests had to be compromised, as well as alternative control strategies when modelling of the selected SMP proved to have limited impact.

4.2 SMP Prototyping

4.2.1 Heating circuit manufacturing

Pattern Design

The process of designing the patterns was done in eagle. The main design idea behind the patterns can be seen in figure 13. They all share the thicker pads in order to facilitate robust soldering. The thicker wire, oriented to the bottom of each pattern design, has lower lower resistance. As a consequence, a lower temperature can be maintained outside the heating zone of the prototype's hinge while keeping the soldered wiring in one place.

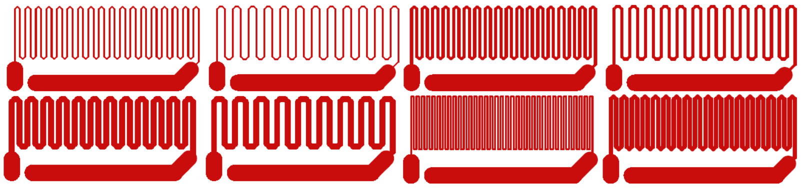

Figure 13: Heating circuit patterns

The purpose of varying the thickness of the copper wire is to find a configuration that works well in the prototyping stage. The thinner the wire, the higher resistance and temperature, according to the illustration in figure 14.

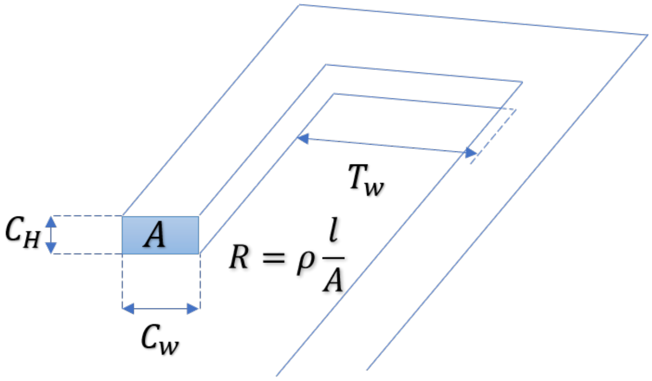

Figure 14: Heating circuit trace

Manufacturing

There are several ways to manufacture a PCB. One common solution today is to mill a copper clad laminate sheet, removing conductive areas to form traces.

The issue with this method is that the milling process is optimized for 1.6mm thick laminates, whereas the pyralux sheet is $85um$ thick. Since the pyralux sheet also isn't completely stretched and flat due to its thin design, acting more like a foil, the milling process risks to cut through the entire sheet and thus destroying the PCB. This is therefore not a very stable way of manufacture for this application.

Another solution is to transfer the pattern to the laminate and etch away the copper that is not covered by the pattern. This has previously been the standard of PCB manufacturing and is used in the industry for mass production. The first step to transfer the pattern can be done in several ways, where the four strategies listed below had to be tried to end up with a stable process.

- Direct printing - Suggested by the importing company "Scan Kemi". Not successful in inkjet or laser printer. Nothing sticks to the copper, the intended print get stuck on the drum and adheres on a later printed part of the paper.
- Toner Transfer - Generally regarded as a simple method and commonly used, but with low precision. Uneven transfer results are often repaired by marker pens, which will ruin the repeatable process the project aims for.

  Attempts were not successful when printed on transparent film with laser printer, and then ironed. Laminate was sanded and rubbed with scotch brite, then cleaned with acetone. Not even a sign of ink transfer could be seen.
- Photo-resist method - Previously used by the institution. One drawback is the introduction of even more corrosive fluids than the etching solution. The method is done as follows: Spray positive photoresist on the copper laminate, as these flexible laminates are not available with pre-coated versions. Print the positive pattern on transparent OH film. Expose the copper laminate in a UV chamber, with the printed OH film as a mask. This dissolves the photoresist in all other places than the circuit trace. Develop the copper laminate with potassium hydroxide, to create the circuit trace on the laminate. This is the previously mentioned chemical which is strongly basic and therefore very corrosive.

  Attempts were not successful with the supplied equipment.
- Laser Cutting - The strategy is to coat the copper laminate in a black spray paint, then burn away the negative patterns to leave a mask of paint over the circuit trace. The chosen laser cutter Epilog Fusion 75W

has a resolution of 600 dpi, resulting in a 1.6 mil trace width. Fiber laser is supposed to be used [4], but as it was not available on this machine, CO2 laser was used instead.

Successful attempts were done with the printer settings in fig 15, using the raster (engraving) mode with a speed of 25% and power of 40%. Reducing the speed results in greater accuracy, for which the power needs to be reduced proportionally for an equally intensive machining. Best result achieved when doing the cutting three times on this low power, to not heat up the laminate too much and reducing the risk of starting fires. Due to the non-flat surface, there was a need to adjust the focus (the height of the table) to burn away the paint in the cavities. Results from the second experiment can be seen in figure 16.

An important note should be made regarding the choice of spray paint. This method was initially disregarded when the following etching process was unsuccessful. The etching process was prolonged from an expected 15 minutes to several hours, when the trace was etched away together with the surrounding copper. It took long time before it was concluded to be because of the choice of a glossy spray paint that the etching did not work. Repeated attempts with matte spray paint was the breakthrough that led to the success of this method.

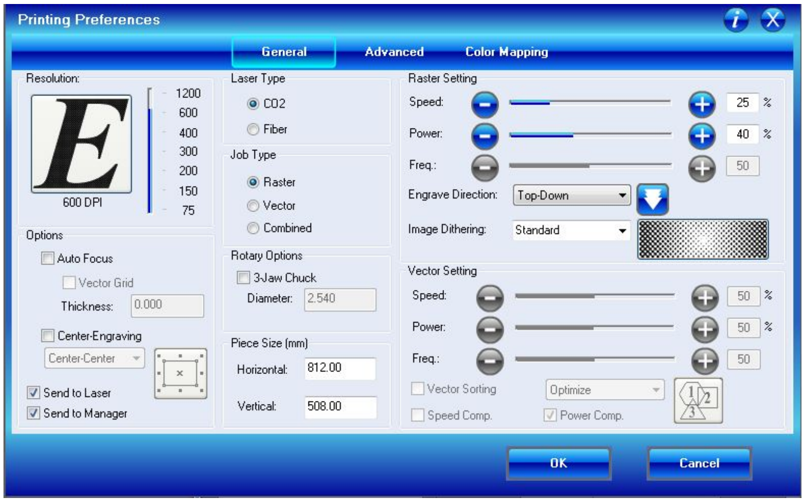

Resolution: 600 DPI

Laser Type
● CO2
○ Fiber

Job Type
● Raster
○ Vector
○ Combined

Raster Setting
Speed: 25 %
Power: 40 %
Freq.: 50
Engrave Direction: Top-Down
Image Dithering: Standard

Options
☐ Auto Focus
☐ Vector Grid
Thickness: 0.000
☐ Center-Engraving
Center-Center
☑ Send to Laser
☑ Send to Manager

Rotary Options
☐ 3-Jaw Chuck
Diameter: 2.540

Piece Size (mm)
Horizontal: 812.00
Vertical: 508.00

Vector Setting
Speed: 50 %
Power: 50 %
Freq.: 50
☐ Vector Sorting
Optimize
☐ Speed Comp.
☑ Power Comp.

Figure 15: Printer settings

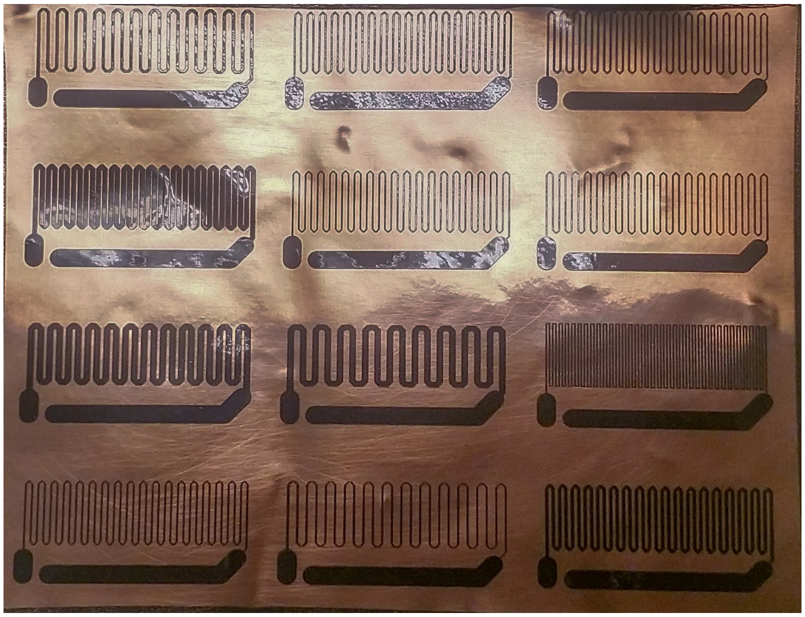

Figure 16: Laser cutting results

Following the pattern transfer is the etching process. 200g Sodium Persulfate was mixed with water in an etching tank, heated to 50 ° C with an immersion heater. The solution was agitated by a stream of bubbles from a bubble tube, shown in action in figure 17. With a properly transferred pattern, the process takes about 15-20 minutes to perform. As the film is translucent, it is easy to see when the copper layer is etched away.

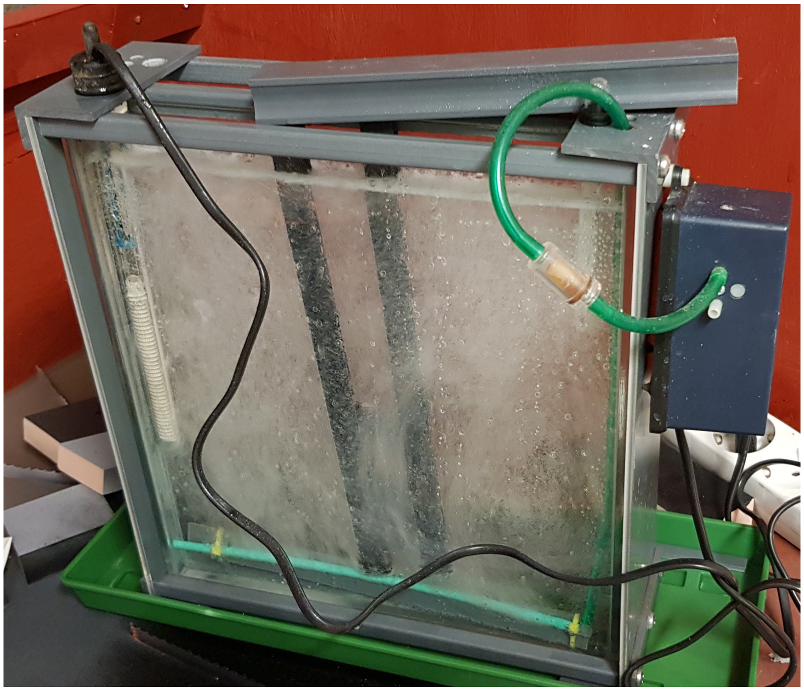

Figure 17: Etching process

The results can be seen in figure 18. The thin traces with circuit width 0.25 mm are clearly damaged, while those with circuit width 0.50 mm shows the lower limitations of this manufacturing method. This also applies to the trace width gap between the traces, which can not be made smaller than 0.50 mm. A circuit width of 0.75 mm shows to be the most reliable way to produce the circuits, but a trace width of 0.50 mm is still achievable.

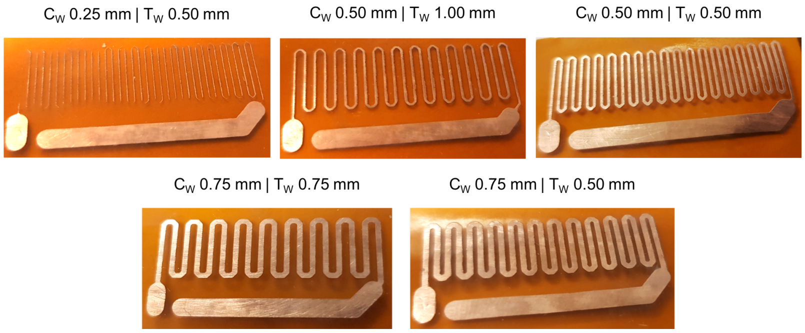

C_W 0.25 mm | T_W 0.50 mm

C_W 0.50 mm | T_W 1.00 mm

C_W 0.50 mm | T_W 0.50 mm

C_W 0.75 mm | T_W 0.75 mm

C_W 0.75 mm | T_W 0.50 mm

Figure 18: Etched copper traces

4.2.2 Prototype cutout

In line with repeatable manufacturing, both the paper substrate and the SMP was cut with laser cutter to reduce prototype variance. The SMP responded surprisingly well to the laser cutting, with minimal deformation, however direction dependent. The machine evidently moves slower in one direction, due to the machine design, which makes the SMP shrink 0.5 mm extra. This was easily accounted for, and the slight melting from this machining stage did not affect the SMP's ability to deform during the tests.

To make the bending process easy, and without manual pre-bending of the paper substrate, a perforation like the one shown in figure 19 was engraved with the laser cutter.

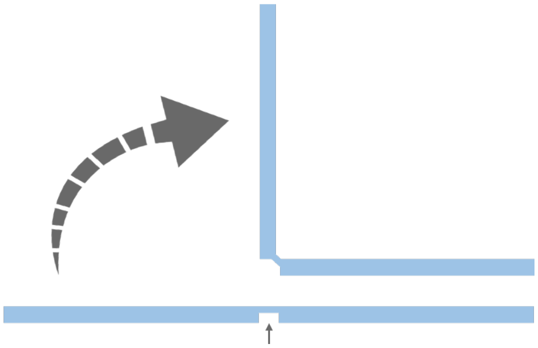

Figure 19: Laser perforation in paper

This was done in the same process as the cutout to ensure accuracy, with two different laser cutter settings for the perforation and the cutout, controlled with color coded lines. The process was prepared in Adobe Illustrator, with the printer settings shown in figure 20.

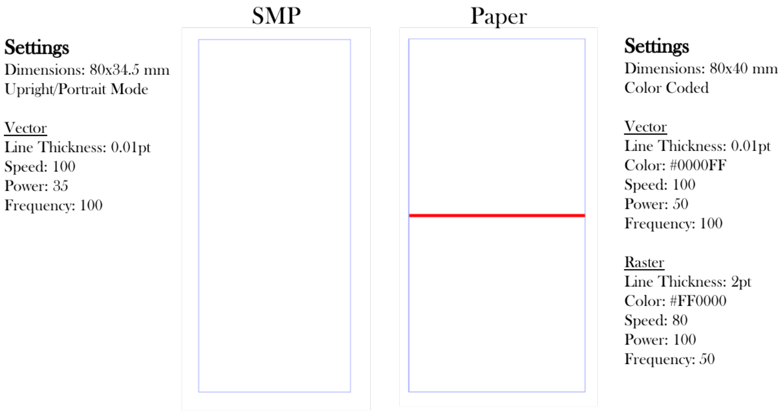

Settings
Dimensions: 80x34.5 mm
Upright/Portrait Mode

Vector
Line Thickness: 0.01pt
Speed: 100
Power: 35
Frequency: 100

Settings
Dimensions: 80x40 mm
Color Coded

Vector
Line Thickness: 0.01pt
Color: #0000FF
Speed: 100
Power: 50
Frequency: 100

Raster
Line Thickness: 2pt
Color: #FF0000
Speed: 80
Power: 100
Frequency: 50

Figure 20: Laser cutting settings

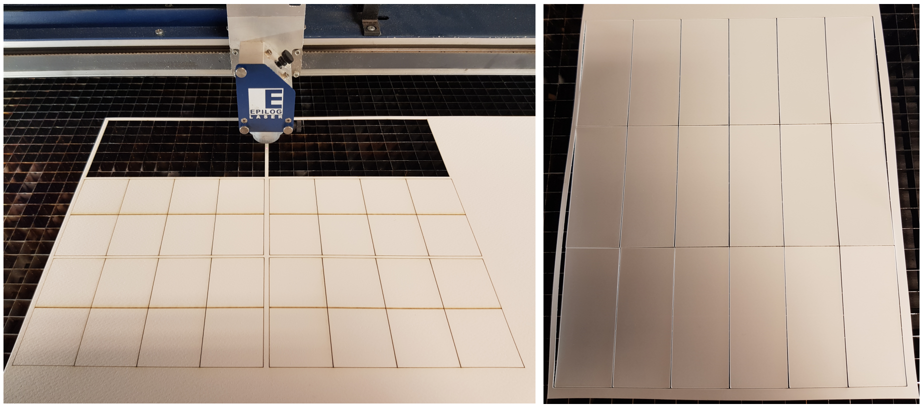

(a) Paper cutouts

(b) SMP cutouts

Figure 21: Laser cutting of prototype components

4.2.3 Prototype Building

With all parts cut out, the prototype was assembled according to figure 22. This structure was experimentally found, where initial tests had issues to get the prototype to bend. Therefore, the stronger shrink film with a shrinkage to 20% to always be used. Another adaption was to not put the tape between the heating circuit and SMP, to allow for relative movement. With the same motivation, it was necessary to leave a 10 mm gap from the hinge free from tape, to ease the bending process. The heating circuit with a 0.75 mm circuit width and 0.50 mm trace width was selected as the standard component, enabling the sufficient heating within current limitations with a reliable manufacturing process.

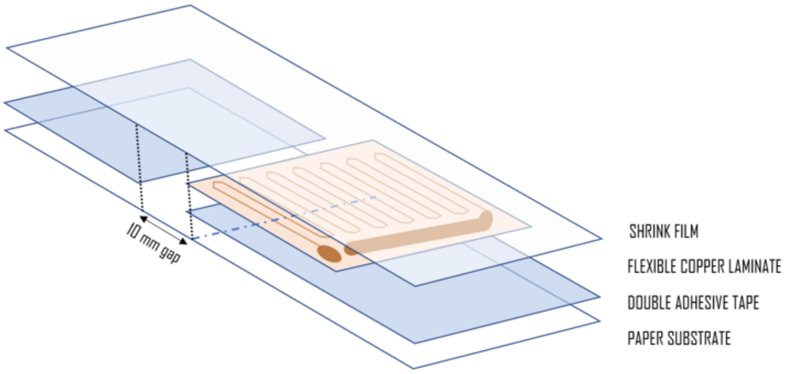

Figure 22: SMP layered prototype

4.3 Bucky Gel Manufacturing

4.3.1 Production Process

The production process of Mukai et. al. [10] lays as a foundation for this part of the project. Following is the list of materials needed, which was ordered from Sigma-Aldrich, and the fabrication steps.

Materials

- Single-Walled CNTs (carbon Nanotube)
- EMIMBF4 (1-ethyl-3-methylimidazolium tetrafluoroborate) as an internal IL
- PVDF (polyvinylidene fluoride)
- DMAC (dimethylacetamide)

Fabrication steps

BGA electrode layer: Contains 22 wt % CNT, 43 wt % ionic liquid and 35 wt% PVDF.

1. Mix 50mg of SWCNTs, 100mg of EMIBF4 in 1ml DMAC together.
2. Ball-mill for 30min at 200rpm.
3. Add a solution of 80mg of PVdF in 2ml DMAC.
4. Ball-mill for 30min at 500rpm.

5. Add 1ml DMAC and be sonicated in ultrasonic bath for 3h.
6. Add DMAC 5ml to get casting solution.
7. Cast in silicon rubber molds and cure in an oven for 12 h at 50 ° C.
8. Put the samples in a vacuum oven at reduced pressure for another 100h in order to let DMAC evaporate completely.

BGA electrolyte layer:

1. Mix EMIMBF4 and PVDF together (1:1 ratio).
2. Dissolve the above-mentioned chemcials in DMAC.
3. Cast the solution similar to the electrode layers.

Fabrication method of actuator film:
The final actuator is achieved by hot-pressing the electrode and electrolyte layers. The thickness of Bucky Gel actuator can decided by the number of electrode layers. The Bucky-gel actuator of $95\mu m$ and $465\mu m$ in thickness by Mukai [10] were fabricated by hot-pressing one Electrolyte(Ey) layer sandwiched by one each electrode(Ed) layer and one Ey layer by five each Ed layer.

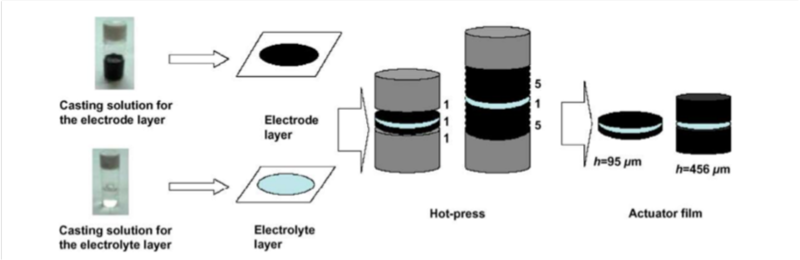

Figure 23: Schematic drawing of the preparation method of the Bucky Gel actuator by hot-pressing the electrolyte film sandwiched by two electrode films

The ball-mill step can be replaced by ultrasonic bath during the making of the electrode layer, but the ball-mill method is more homogeneous. The main idea is that the electrode solution gets evenly mixed.

4.4 Sensor Implementation

4.4.1 Computer Vision Algorithm

The Computer Vision algorithm had two main objectives, image capture and angle calculation from collected image data. As was mentioned under project design, image capture was performed using a Logitech C920 Web Camera connected directly to the Raspberry Pi, where the image processing and eventual angle calculation was performed. The preliminary output of an early implementation of the algorithm (applied on a single hinge design) can be seen in figure 25, with the input image shown in figure 24. The markers are picked up as bodies and sorted based on their distance from the bottom-left corner of the image. The relevant angle is then calculated using simple trigonometry. For the double hinge design, the distance from the top-left corner was used instead.

For a time during the implementation process, there was an alternative solution to sorting the bodies in the double hinge design being considered. The argument was made that should the prototype overshoot its target angle by a large magnitude, some markers would incorrectly end up closer to the point of reference than other markers, making the algorithm misidentify the bodies. A solution was being developed for this, where the bodies' positions from the last loop-iteration were saved and pair-matched to the bodies of the subsequent sample. However, this solution was abandoned since the overshoot needed for the aforementioned problem to occur practically never happened, and the pair-matching with the previous sample then only served to introduce a potential instability in the algorithm (I.E. one faulty sample cycle could potentially cause the script to misidentify the bodies for the rest of the run).

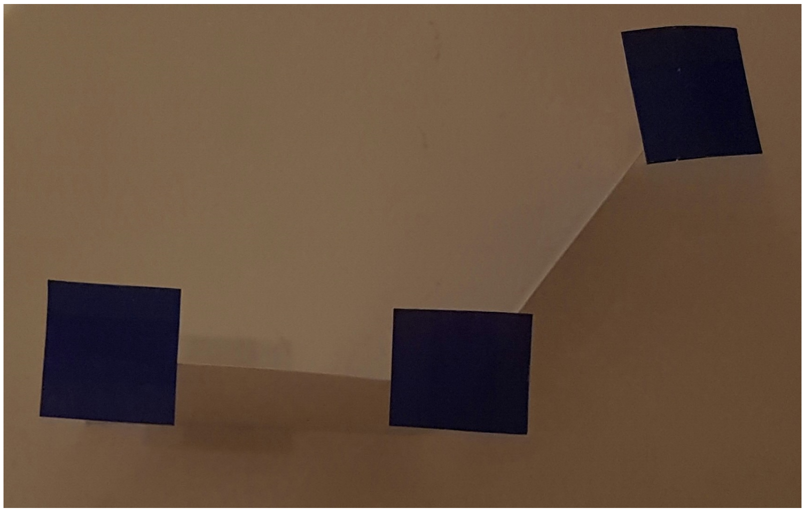

Figure 24: Computer vision markers

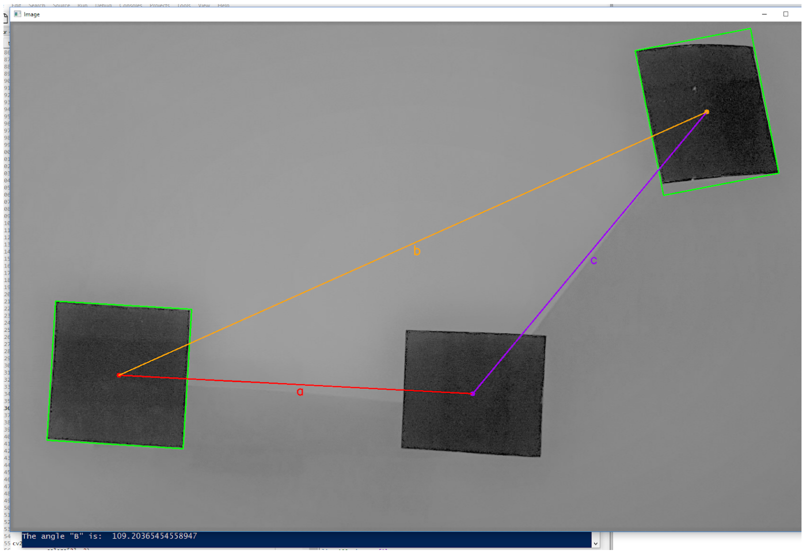

```
The angle "B" is:  109.20365454558947
```

Figure 25: Computer vision angle detection

The CV-algorithm was implemented using the OpenCV package in python 3, primarily favored for its ease of use, relative simplicity in implementation and easily accessible documentation.

The image processing itself was performed through 6 major steps (also see figure 26):

- Convert to Grayscale: A multitude of functions in OpenCV expects grayscale images, and will implicitly convert input images to it. Since the algorithm does not use specific color detection, it saves time and processing power to only do this once at the start of the process.
- Image Smoothing: Convolving the image with a Gaussian kernel, reducing noise.
- Image Thresholding: A side benefit of using the aforementioned marker-based solution is that one can set a threshold value, and then iterate over all the pixels in the image, setting them to either white or black depending on which side of the limit they fall. This massively reduces the sensitivity to lighting variations in the test environment.
- Canny Edge Detection: Calculates the edge gradient of every pixel in the image and filters them out if they don't constitute a local maximum, leaving a binary image with "thin" (one pixel wide) edges. Finally, Hysteresis Threshold calculations are performed on the edges, saving or discarding them based on intensity gradient and connectivity.

- Contour Detection: A contour in OpenCV is defined as a curve joining all the continuous boundary points having the same color or intensity (within a specified tolerance). Since the shape of the bodies to be detected is known to be squares, only the coordinates of the corner points are saved and passed to the next part of the script.
- Calculation: The sought angles are calculated using the midpoints of the bodies captured in the previous step. The information is communicated and the algorithm waits for a new measurement cycle to begin.

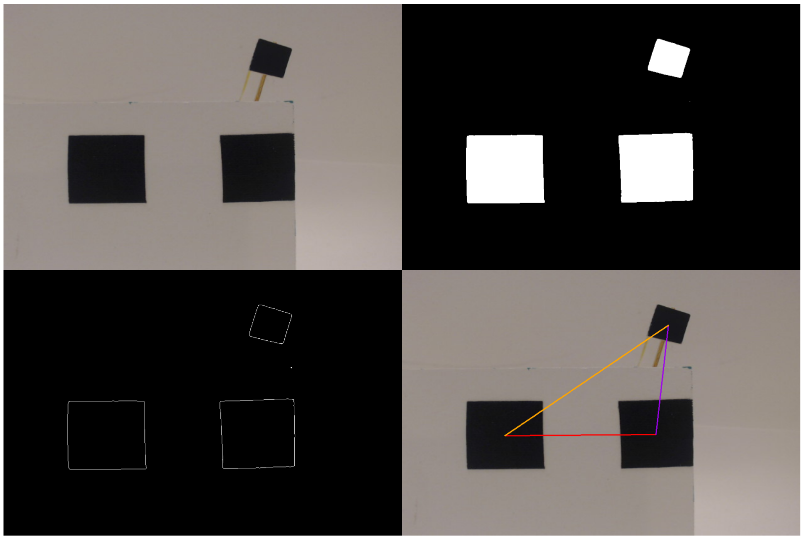

Figure 26: Computer vision process. From top left to bottom right: Base Image, Thresholding, Edge Detection, Calculation.

There are two main factors that impose an upper limit to the sampling frequency: the maximum capture frequency of the camera with included communication time to the controller and the processing speed of the hardware used for the implementation of the algorithm. Regardless, for the monitoring of the SMP-hinge, it was deemed that the system was sufficiently slow for this not to be of any major concern.

The accuracy of the angle measurement is limited by how precisely the marks in the corners of the hinge can be placed, and the resolution of the image capture. Increasing the resolution will increase the accuracy of the measurements (though at vastly diminishing returns at high resolutions), but will decrease the sample frequency, both from communication time (larger data packages) and processing time (exponentially more pixels to iterate over).

4.4.2 Thermal Sensor

The chosen sensor has an internal EEPROM storage where it stores the temperature values of each pixel in the 16x4 array as well as the ambient temperature. The values are between 15-18 bits each. This also means that the amount of data needed to be accessed by a microcontroller would be 15*64 + 15 = 975 bits at the very least. Individual values of the sensor can be read by accessing specific addresses on the sensor.

Figure 27 shows how the sensor was connected to the Arduino. The serial communication allows for measurement transmission every 50 milliseconds, while the sensor is able to read every millisecond. The Arduino therefore averages 50 samples for each transmission, which reduces the sensor noise.

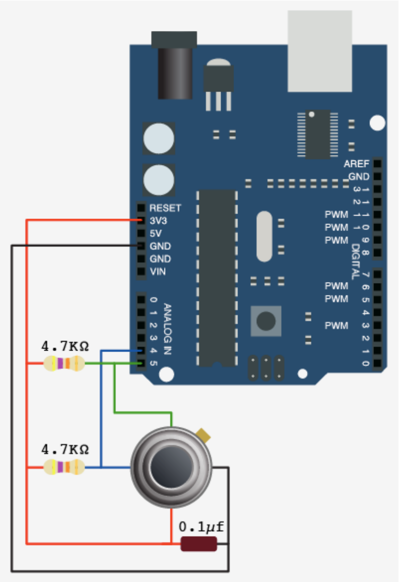

Figure 27: Thermal sensor connections

The mounting of the sensor can be seen in figure 28, where a 3D printed design with microservos was chosen to enable multiple hinge measurements. The sensor could then be redirected automatically, reducing the number of sensors needed.

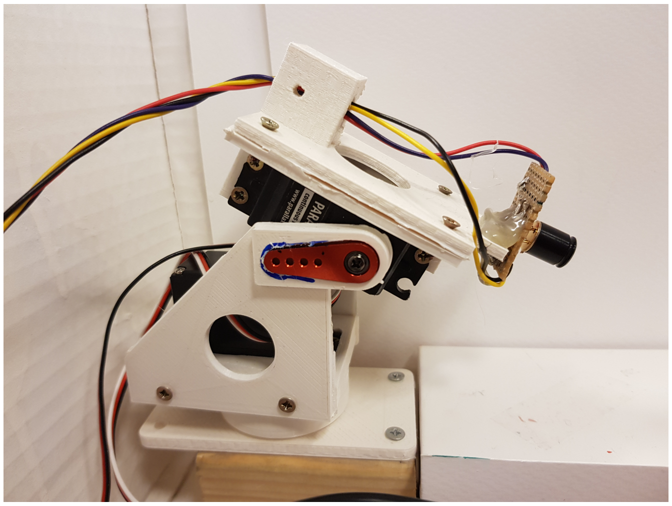

Figure 28: Thermal sensor with 3D printed setup

The thermal sensor used has a field of view of 60° in the horizontal plane, and 16° in the vertical plane. The sensor measures the temperature in an orthogonal contact plane, relative to the sensor, in which it has a resolution of 16x4 pixels. As such, the distance between the sensor and the measured object will define the area which one pixel covers, shown in figure 29.

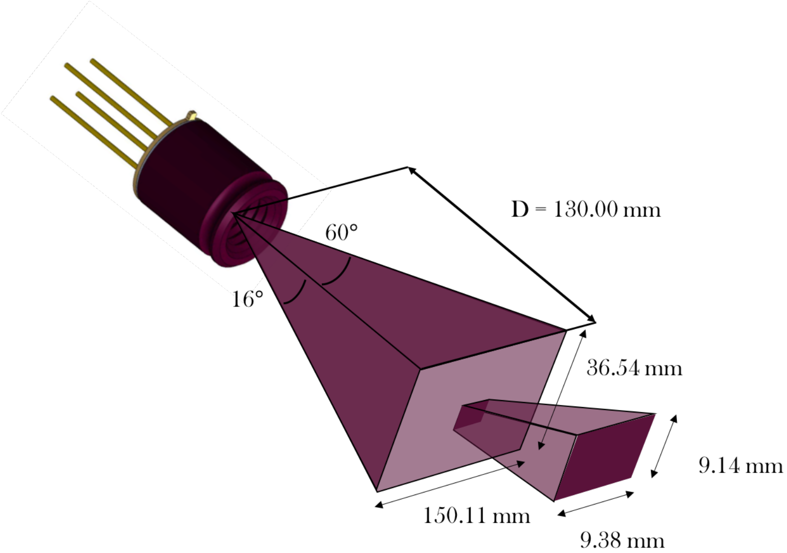

Figure 29: Thermal sensor position

With a 13 cm distance between the sensor and the heating element, as it was initially set up, the pixel area is about 1x1 cm. The dimensions of the heating element is 3.8x1 cm, which means that in the ideal case, the pixel area covers the full heating element exactly. However, at a slightly different angle, the pixel area will effectively cover parts of the heating element and part of the surrounding material of a lower temperature, which will distort the sensor readings, as shown to the left in figure 30. This was verified with a more exact, but handheld Flir thermal camera, where a clear deviation was shown between the thermal camera and the sensor at higher temperatures, but not at the initial room temperature.

The solution to this was to bring the thermal sensor closer, so that in worst case there still has to be a full pixel value covering only the heating element. This is shown to the right in figure 30, where the worst case is concluded to be where two pixels fully cover the heating element. As such, the maximum allowed pixel width x_c is 5 mm, resulting in a maximum distance of 71 mm between the sensor and the hinge. As the sensor was moved to this position, the thermal sensor could be verified to be working with the Flir thermal camera.

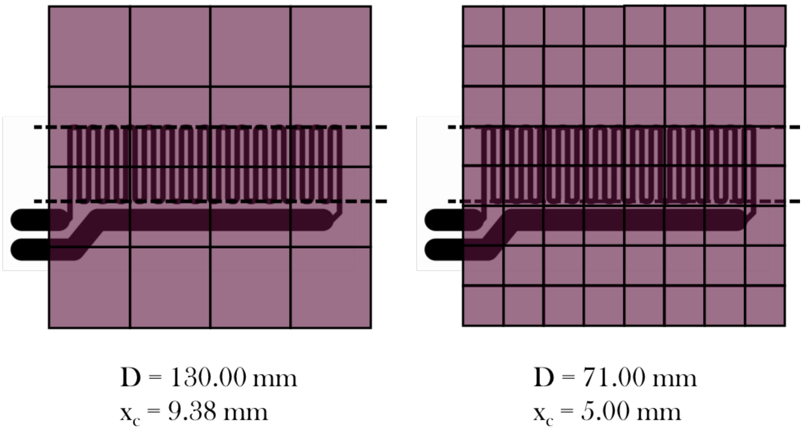

Figure 30: Thermal sensor pixel width

4.4.3 Current Sensor

In figure 31 is a simple schematic to connect this device to the Arduino. In this case, a motor is used as a load and batteries as the supply. In the case of the SMP, the current driver acts like the supply, and the SMP is the load. The difference between using a simple battery and a MOSFET current driver that uses pulsed DC is that the sensor needs to be calibrated to read a pulsed DC signal. The DC signal from the MOSFET has a certain frequency, which in this case is 1000 Hz. Depending on the frequency at which the sensor values are being read, the results can have a large variance. While using the setup with the SMP, the current sensor reads 50 values over the course of 50 ms and averages them to reduce this variance and to reduce sensor noise.

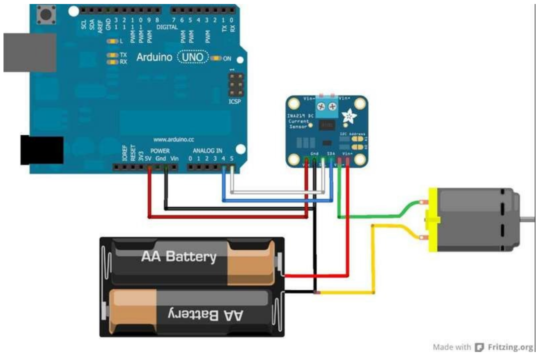

Figure 31: Current sensor schematic

4.5 Electronics

4.5.1 Current Driver

The components for the custom made current driver were selected with cost and utility in mind. A complete list of the components is disclosed in Table 3.

Type	Requirement	Component
MOSFET	High current, low resistance when on, opens predicably at +12V	IRF2804PBF - MOSFET N, 40 V 75 A 300 W TO-220 - IR
Transistor	Opens predictably at +3.3V	Small signal transistor E-Line PNP
Resistance	Allow a small current from the microcontroller	1kOhm standard resistor
Diode	Robustness	Zener diode, 1N5351BG, 14V 5W

Table 3: Component list for the PWM current driver

The main component of the current driver, a MOSFET transistor, was selected to sustain large currents, i.e. $R_{DS,on} << R_{load}$. The design idea that was realized was to use the MOSFET transistor directly connected from drain to the load (i.e. the copper circuit) and from source to the ground. The gate was to be controlled by a PWM signal from the Arduino microcontroller. However, a ±12V signal was required to reliably open the gate of the

MOSFET, while the microcontroller had a supply voltage limitation of 3.3V. In order to allow PWM signal switching of the MOSFET transistor with this configuration, a smaller transistor was added and controlled by the microcontroller, draining the 12V supply to ground when it is open. When it is closed, the 12V supply will open the gate of the MOSFET transistor and thereby allowing the large current through the load. Thus, the microcontroller PWM will have an inverted effect on the MOSFET transistor. The final schematics for the current driver can be found in figure 32.

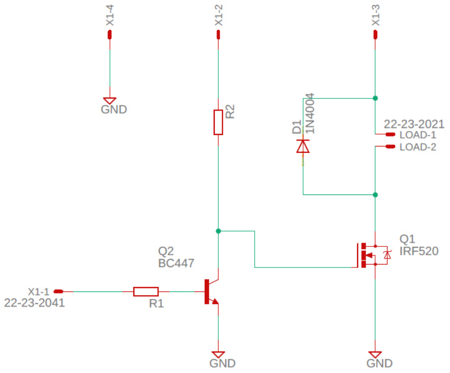

Figure 32: Current driver schematics

The current driver was manufactured using the milling method on a dual-layered 35μm copper laminate sheet. The complete rub out setting was used, thus all excess copper was removed. This setting makes the current driver PCB more robust and additionally, it facilitates soldering the components. The results of this manufacturing procedure can be found in figure 33.

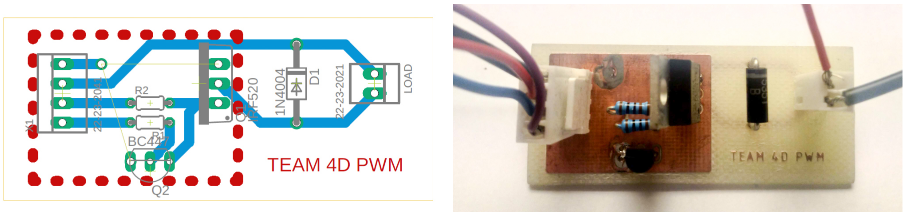

(a) Eagle board design

(b) Manufactured current driver

Figure 33: Current driver

4.5.2 Complete Printed Circuit Board

A preliminary breadboard design was first realized in order to assess the functionality of the electronics system. An overarching illustration of the electronics, circuitry and the included components in the breadboard design can be found in figure 34.

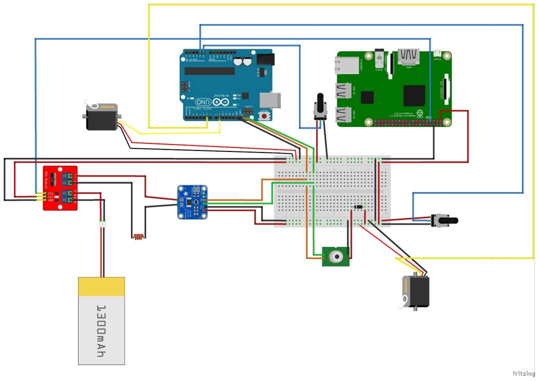

Figure 34: Conceptual schematic

In order to reduce cabling and to make the system easier to manage and more robust against disturbances and human errors, a PCB was designed in Eagle. Additionally, the aforementioned current driver was integrated in the PCB to reduce the amount of separate components. The PCB schematic is depicted in figure 35.

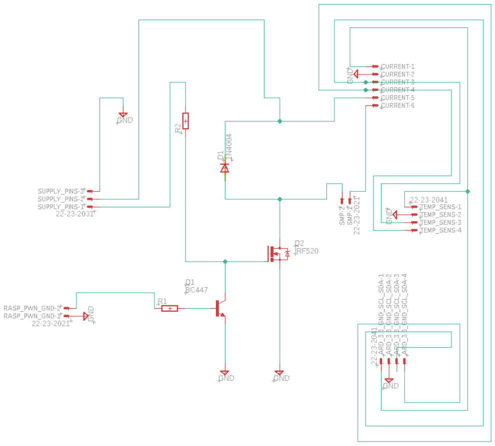

Figure 35: Eagle schematic

Moreover, a requirement for the complete system was that it had to handle the heating of two separate hinges (for the dual-hinge SMP prototype). Given the incumbent sensor setup described in Section 4.4, heating of the two hinges could not be done concurrently. Additionally, sequential heating was deemed sufficient for the purposes of this project. The switching between the two hinges for the double hinge design was done with an external ON-ON toggle switch that could tolerate large currents. The switch was conveniently mounted on the edge of the test chamber box.

The PCB was manufactured using the milling method on a single-layered $35\mu m$ copper laminate sheet. Similarly to the current driver and according to the same reasoning, the complete rub out setting was used. The final board using this method is displayed in figure 36.

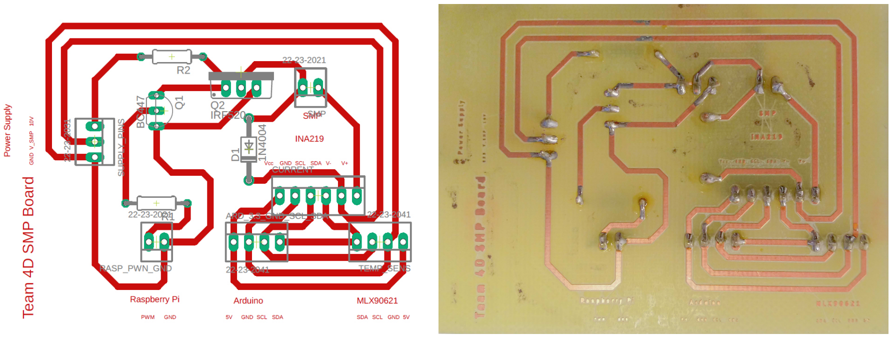

(a) Eagle board design

(b) Manufactured PCB

Figure 36: Printed circuit board

4.6 System Integration

I2C interface and Arduino

As both an Arduino and a Raspberry Pi was used, there was a need for serial communication between the devices. The I2C communication bus is very popular and broadly used by many electronic devices, because it can be easily implemented in many electronic designs which require communication between a master and multiple slave devices or even multiple master devices. The easy implementations comes with the fact that only two wires are required for communication between up to almost 128 (112) devices when using 7 bits addressing and up to almost 1024 (1008) devices when using 10 bits addressing.

Each device has a preset ID or an unique device address so the master can choose with which devices it will be communicating.

The two wires, or lines are called Serial Clock (or SCL) and Serial Data (or

SDA). The SCL line is the clock signal which synchronizes the data transfer between the devices on the I2C bus and it's generated by the master device. The other line is the SDA line which carries the data.

The two lines are "open-drain" which means that pull up resistors needs to be attached to them so that the lines are high, because the devices on the I2C bus are active low. Commonly used values for the resistors are from 2K for higher speeds at about 400 kbps, to 10K for lower speed at about 100 kbps.

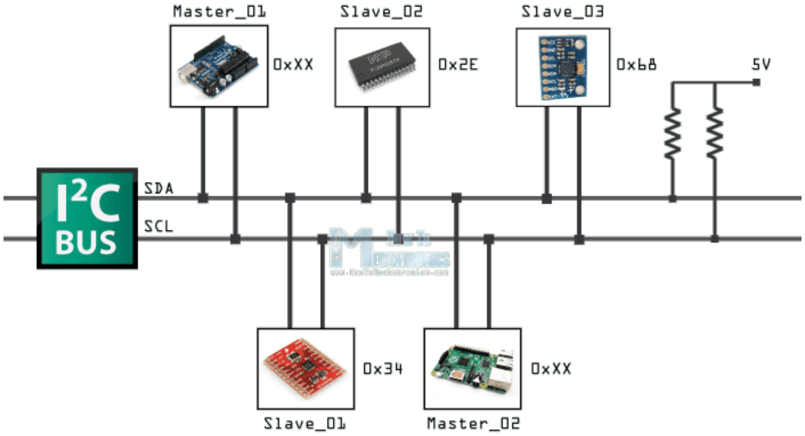

Figure 37: I2C Communication

The data signal is transferred in sequences of 8 bits. So after a special start condition occurs, the first 8 bits sequence comes, which indicates the address of the slave to which the data is being sent. After each 8 bits sequence, a bit follows that is called Acknowledge. After the first Acknowledge bit, in most cases another addressing sequence comes but this time for the internal registers of the slave device. After the addressing sequences, the data sequences follows as many, until the data is completely sent and it ends with a special stop condition.

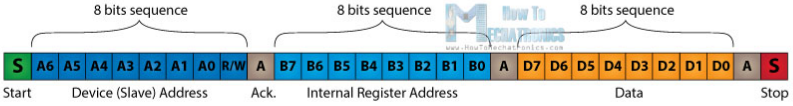

Figure 38: I2C Bit Sequence

The start condition occurs when data line drops low, while the clock line is still high. Thereafter the clock starts and each data bit is transferred during each clock pulse.

The device addressing sequence starts with the most significant bit (MSB) first and ends with the least significant bit (LSB) and is actually composed of 7 bits, because the 8th bit is used for indicating whether the master will write to the slave (logic low) or read from it (logic high).

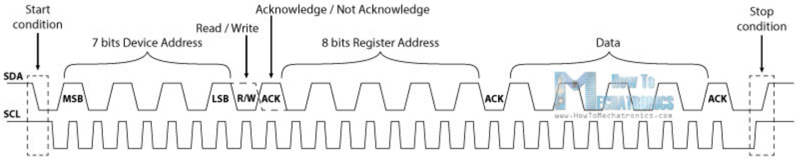

Figure 39: I2C Message

The next bit ACK/NACK is used by the slave device, to indicate whether it has successfully received the previous sequence of bits. At this time the master device hands the control of the SDA line over to the slave device and if the slave device has successfully received the previous sequence, it will pull the SDA line down to the condition called Acknowledge. If the slave does not pull the SDA line down, the condition is called Not Acknowledge, and means that it did not successfully receive the previous sequence, which can be caused by several reasons. For example, the slave might be busy, not understand the received data or command, or cannot receive any more data and so on. In such a case the master device decides how it will proceed.

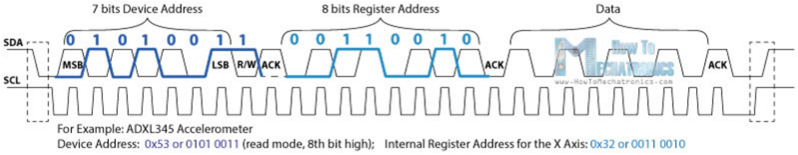

For Example: ADXL345 Accelerometer
Device Address: 0x53 or 0101 0011 (read mode, 8th bit high); Internal Register Address for the X Axis: 0x32 or 0011 0010

Figure 40: I2C Addressing

Next is the internal registers addressing. The internal registers are locations in the slave's memory containing various information or data. The sensor has an unique device address and addition internal registers addresses, for the sensor data. To read this specific sensor data, the device address needs to first be sent, followed by the particular internal register address for the chosen data. These addresses can be found from the datasheet of the sensor.

After the addressing, the data transfer sequences begins either from the master or the slave, depending of the selected mode at the R/W bit. After the data is completely sent, the transfer will end with a stop condition which occurs when the SDA line goes from low to high while the SCL line is high.

4.7 Modelling

To develop a control design that achieves a desired angle the system needs to be modelled. The modelling was divided into two parts, one that includes all the sensors and is more complex and the other part scales down the complexity by excluding the temperature sensor, which results in a cheaper control design. The more complex model is a state-space model with the two states temperature and angle where the input is current. The less complex model is based on the angular velocity to predict the final angle.

For the complex model the system was considered to be a black box estimation, where the state-space model is desired with two states. There are three Matlab commands for estimation of the state-space models: ”ssest”, ”ssregest” and ”n4sid”. The estimation method ”ssest” is a iterative estimation that obtains maximum-likelihood values by minimizing the prediction errors. The estimation methods ”n4sid” and ”ssregest” are non iterative subspace estimators, [13] where ”ssregest” estimates by reduction of regularized ARX model [15] and ”n4sid” use subspace method [14]. For the estimation commands, the data output signals temperature and angle was modified to have the initial values at zero and the order was chosen to two. Thereafter all the three methods mentioned could be simulated in Simulink and used to compare with the real gathered data and finally choose the most suitable method. Eventually a discrete-time identified state-space model can be obtained, see equation 1 and 2.

$$x(t+Ts) = Ax(t) + Bu(t) + Ke(t) \tag{1}$$

$$y(t) = Cx(t) + Du(t) + e(t) \tag{2}$$

A,B,C and D are the state-space matrices and K the disturbance matrix. The input is represented as $u(t)$, the output $y(t)$, the vector of states $x(t)$ and the disturbance $e(t)$. For this project the disturbance was neglected and the D matrix was set to zero by default.

For the less complex model the angular velocity was obtained taken the average velocity of two samples according to equation 3.

$$velocity = \frac{angle_{i+1} - angle_i}{time_{i+1} - time_i} \tag{3}$$

Thereafter the angular velocity was smoothed using a 5-point moving average. The final angle, final angular velocity and the angular velocity when current was cut off can be obtained approximately by reading from the plots. Thereafter the prediction model could be used for the control design.

Another investigation for the modelling was to compare the temperature of the SMP and the copper circuit. To obtain the temperature of the SMP a temperature sensor was used. Furthermore the changing temperature of the copper was obtained by observing the changing resistance. To obtain the resistance R, the voltage, U and current, I was measured with a current sensor. Hence, the resistance of the copper circuit was achieved from Ohm's law, see equation 4.

$$R = U/I \tag{4}$$

The resistance of the copper changes with temperature according to equation 5.

$$R = R_{ref}[1 + \alpha(T - T_{ref})] \tag{5}$$

The variable R is resistance of the copper at its temperature T, R_{ref} is resistance of the copper at its reference temperature T_{ref} (usually 20° C), where α, the temperature coefficient of resistance for the copper, is specified at. The coefficient α for copper is 0.004041. The temperature of the copper is given by factoring the variable T in equation 5.

4.8 Control Design

The target of the controller was to make the bending SMP stop at a certain angle. To achieve this, a data-driven model was generated and was used for angle prediction.

The controller was monitoring the status of the SMP and predicting the optimal time to cut off the current at each sampling time.

SMP hinges are difficult to model by transfer function or state-space model due to its nonlinear behavior. During the bending process, The transfer function of the system changes significantly with temperature and angle. To this end, we decided to have a fixed current input for all experiments and prototypes to ensure different SMPs have similar behavior. Also, the control signal in this case was only ON/OFF signal.

A receding horizon model-predictive control algorithm was implemented in the Simulink.

To implement a MPC controller, an optimization problem is defined:

$$\begin{aligned} \underset{u^*}{\text{minimize}} \quad & V = x_N^T P x_N - x_{ref}^T P x_{ref} \\ \text{subject to} \quad & x_0 = \mathbf{x}, \quad \textit{initial} \quad \textit{state}, \\ & x_k = A x_{k-1} + B, \quad k = 1, \ldots, N, \\ & u_k = 0, 1, \quad k = 0 \ldots, N-1, \\ & u_i = 0, \quad u_{i-1} = 0, i = 1, \ldots, N, \\ & A = A_1, B = B_1, \quad u_k = 1, \\ & A = A_2, B = B_2, \quad u_k = 0 \end{aligned} \tag{6}$$

Here V is cost function, P is the terminal state weight, N is the control horizon, x is state vector, u is control(input) vector, u* is the optimal control input sequence $[u_0, ..., u_N - 1]$ that minimize the cost function.

The cost function V that needs to be minimized only depends on the final state x_N. x is a state array containing two variables, temperature and angle . x_{ref} is the reference value, in this problem, only reference angle was used.

$P = \begin{bmatrix} 0 & 0 \\ 0 & 1 \end{bmatrix}$, which means only the deviation of the second final-state variable is evaluated, which is the angle of SMP.

Input vector is a binary signal, 1 refers to the current is on and 0 is off. Also, Two different state-space models A_1,B_1 and A_2,B_2 were used for heating and cooling process.

The fourth constraint implies that once the current was cut off, it will not be turned on for the rest of time i.e. the power supply only switch once.

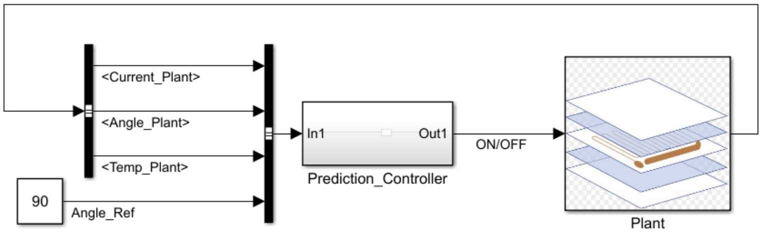

Figure 41: Control structure

Figure 41 shows the control structure of the embedded system.Due to time limitation and hardware limitation, MPC controller was not used for the real prototype. Instead, a heuristic approach was used for predictive controller.

A linear function replaced the state-space model for prediction. Instead of predicting the optimal cut off time, the practical controller predicted the final angle of the SMP assuming the current was cut off at the end of the current sampling time. If the predicted angle exceeded the reference angle, the current will be cut off at the end of the sampling time.

5 Verification & Validation

To verify the system performance, subsystem tests was made of all components to make sure that they were operating correctly according to our internal specifications. Following system tests, integrating these subsystems, could validate the system behaviour against the stakeholder requirements.

5.1 Subsystem Tests

5.1.1 Thermal sensor

Testing of the thermal sensor consisted of evaluating the predicted Field of View and accuracy of the sensor through the means of measuring objects of known temperature and by plotting the temperature values in a matrix to give an idea about the Field of View of the sensor.

Testing for the accuracy was done with the help of the Flir Thermal Camera. With it, the temperature of a heating coil (the copper coil used in the experimental setup) maintained at a constant temperature of 200 degree Celsius was measured and the results were compared. At the next level, the distance of the coil from the thermal sensor was varied, beginning at 15 cm till 5 cm in steps of 5 cm and the results were tabulated. Using this data, the resolution of the pixels of the thermal sensor could be determined.

Testing for the Field of View was done by plotting the individual values measured by the sensor in front of it in a matrix form. Color coding the numbers from the sensors helped form a pictorial representation of the pixels of the thermal sensor. By keeping a warm object of known shape (in this case, a square plate at a temperature higher than room temperature of 27 degree Celsius) at a known distance and by looking at the area of the square that was visible in the plot, the Field of View could be determined.

5.1.2 Current sensor

To test the accuracy of the current sensor, a resistance of known value was connected to the sensor as the load and a known voltage was applied across it. This drove a known current through the entire circuit, which was the basis for the test. Resistances of 1, 10 and 100 Ohms were used, with a fixed voltage of 1V applied across them. Since the supply that applied the voltage also contained a well calibrated voltage and current sensor, calibrating the current sensor could also be done.

5.1.3 Computer vision

The performance requirements for the computer vision angular sensor were sufficiently high sampling frequency, low random error/noise and reliability in execution. To verify whether the frequency requirement was fulfilled, the average execution time per measurement loop was used. For verification of noise being sufficiently low, minimum and maximum deviation from a static measurement was used. Lastly for reliability, the percentage of samples where valid measurements were registered (i.e. the correct bodies were detected and properly sorted and identified) was used.

5.1.4 Current driver

The output was first measured and compared to the input and the output noise was measured with an oscilloscope. The current driver was further tested by connecting it to an arduino microcontroller and using a resistance coil of 0.385 Ohms, powered by a supply that drove a current of 2.6 Amperes across the coil. The test was performed by varying the PWM signal generated by the microcontroller from 0% to 100% in 5 steps and the corresponding current through the circuit was measured. A relationship between the PWM and the voltage across the load can be determined this way.

5.1.5 Complete PCB

Testing for the PCB started with verifying the connections on the PCB to determine their robustness. All connected components were then individually tested to determined their functionality when using the PCB. After this, the entire setup was run under experimental conditions that were identical to the testing environment.

In this case, the copper heating circuit was used as a load, the PWM driver that was now on the PCB was used as a way to drive the copper heating circuit, the current sensor was used as a way to measure current and the temperature sensor to measure the temperature of the copper circuit. The same supply was used as in the previous tests. PWM was tested at 50%, 100%, 20%, 80% and 0% duty cycles to determine if the PCB could handle large currents. Then the current through the PCB was varied from 2.6 Amps to 3.0 Amps in steps of 0.1 amps.

5.1.6 Complete Software

The requirement on sampling frequency of the complete software solution was verified by simply measuring the average sample time over a large number of iterations. To verify the synchronization of the measurements, the data was manually reviewed until consistent behaviour was observed enough times to be deemed rigorous.

5.2 System Tests

Single Hinge Design
To validate the single hinge system, there were different experiments conducted that can be roughly divided into two parts. One part when the

current is cut off at a fixed time for all the experiments, which is open-loop controlled and the other part when the current is cut off at fixed angles, which is closed-loop controlled. For the double hinge design there were two interesting final angles at 45° and 90°. Therefore the second part of the experiments was conducted on one hinge with desired angles around the two interesting final angles. To simplify the identification of the system, the current was fixed at 2.6A when it was turned on. Conclusively the testing can be specified and divided into four test cases.

Test case 1
Specified as the first part this test case was made with the cut-off time at 2 min 36 seconds for five experiments.

Test case 2
Specified as the second part, this test case was made with five experiment with different desired angles close to 45° :

- Experiment 1: 40°
- Experiment 4: 42°
- Experiment 2: 45°
- Experiment 5: 47°
- Experiment 3: 50°

Test case 3
Specified as the second part, this test case was made with five experiments with different desired angles close to 90° :

- Experiment 2: 80°
- Experiment 1: 85°
- Experiment 4: 87°
- Experiment 3: 90°
- Experiment 5: 92°

Test case 4
The last test case specified as the second part was also an experiment made five times but the current was cut off when the angle reached a value larger than 42°.

Double Hinge Design

As the bending control was focused on the single hinge design to isolate this behavior, the tests for the double hinge design instead focused on the scalability of the system. As such, the double hinge system tests were not designed with the controller performance in mind, but to focus on the validity of the system design in a more complex context.

First, the material needed to be proven to be strong enough to bend and hold an extended hinge after a perforation. Second, the computer vision system needed to be able to concurrently track more than one angle. Third, the controller hardware needed to be able to use the custom made switch, to change the current driver to actuate the second hinge. This was all tested through a new double hinge arm prototype, based on the concept design.

6 Results

This section covers the results from the project, including learnings from tests.

6.1 Learnings From Tests

6.1.1 Subsystem Performance

Thermal sensor
Test results for the thermal sensor are tabulated in the table 4 below.

Distance from object	Measured Value in Celsius	Actual Value in Celsius
15 cm	163.54	203.21
10 cm	176.98	202.9
5 cm	201.43	203.4

Table 4: Temperature sensor performance

From the test results, it can be seen that the most optimal distance to keep the thermal sensor to get accurate values would be around 5 cm from the test sample. This however, also depended on the surface area of the heated sample. In the case of the copper coil used in this setup, 5cm - 7cm was found to be the optimal distance needed to measure the correct temperature value. An object with a larger surface area would need the sensor to be placed further away and vice versa.

Current sensor
Test results for the current sensor are tabulated below in tables 5

Load in Ohms	Measured current in mA	Actual current in mA
1	952.1	952.38
10	92.7	93.37
100	9.84	9.97

Table 5: Current sensor performance with different loads

From the table it can be seen that the values measured by the current sensor were found to be sufficiently accurate compared to the actual current values.

Computer vision
For the Computer Vision solution, performance measures are observable in Table 6 below.

Measure	Value	Requirement
Sample Time	$0.12s$	$< 0.4s$
Noise	± 0.5 degrees	$< \pm 1$ degrees
Reliability	> 99 %	> 95 %

Table 6: Computer vision performance

These values all fall well within the stipulated requirements.

Current driver

The output signal of the current driver followed the signal input signal according to expectations. The voltage measurements over the coil showed that the voltage was inversely proportional to the PWM's duty cycle, also according to expectations.

Furthermore, an interesting observation was made during the SMP heating experiments in which the current driver was used. The copper heating element was fed with a DC equivalent current corresponding to the previous experiments using a DC supply. Heat radiating from the copper heating element had increased significantly. As a consequence, SMP prototype actuation began alarmingly fast in most cases, while prototypes were burning up in a few other cases. This posed a conundrum for the project group initially as the current sensor was reading the desired DC equivalent current and all else was held equal. In order to solve this conundrum, the fundamental equation for electric power had to be revisited. It was soon figured out that the culprit in this drama was the quadratic relationship between power and current in $P = RI^2$. Given $R = 1\,\Omega$, a duty cycle of 50% and a top value for the current at $2A$, $I_{PWM} = \frac{Imax+Imin}{2} = 1A$. For one period of the square wave, $P_{PWM} = \frac{RImax^2}{2} = 2W$, while for an equivalent $I_{DC} = 1A$, the heat loss will only be $1W$.

While the purpose of a driver circuit often is to drive some kind of load through regulation of e.g. the current, it is rarely the case that the purpose of this regulation is to heat something up. This result may seem obvious *a posteriori* but took some time to troubleshoot. Due to the time constraint of this project, a decision was made to continue experiments using a DC supply. The current driver was subsequently used as a binary switch, accurately switching off the current at the correct angle in closed-loop experiments.

Complete PCB

A multimeter showed that all connections were proper. After subsequently and successfully assessing each component/peripheral separately, the entire system was verified by running experiments mimicking test conditions. All external components/peripherals successfully ran concurrently. Letting the PCB drive the copper heating circuit for various duty cycles, the PCB proved to be robust against large currents. There was no noteworthy heat building up in any of the components, which was assessed with a Flir thermal camera.

Complete software

The average sample time for the complete software solution was observed to be just below 0.6 seconds, which is within the specified requirements, distributed between the different subprocesses as seen in table 7.

Sensor	**Sample Time**	**Requirement**
Thermal Sensor	$< 0.1s$	-
Current Sensor	$0.45s$	-
Current Driver	$< 0.1s$	-
Computer Vision	$0.12s$	$< 0.4s$
Total	**0.57s**	**<0.6s**

Table 7: Distribution of sample time

The overall software solution is within specifications as it relates to sample time. It's also apparent that while the speed could potentially be improved through running the current sensor and the computer vision in parallel (with efficiency depending on RAM limitations), the time saved would be fairly minor, since the current sensors anti-aliasing process is a major bottleneck standing in the way of improving overall sample time.

Manual verification confirmed that the data from the different sensors synchronized properly.

6.1.2 System Performance

Single Hinge Design

In figure 42b, one can see a single hinge prototype with an attached marker, successfully bent. It displays the deformation of the SMP over the heating element in order to bend, which would not have been possible with tape at that location. In figure 42c, one can see the complete test setup, which overlaid sensor data. The current is turned off with PWM duty cycle of 100 and the maximum temperature in view is 108 degrees, with a final angle of 44.19°.

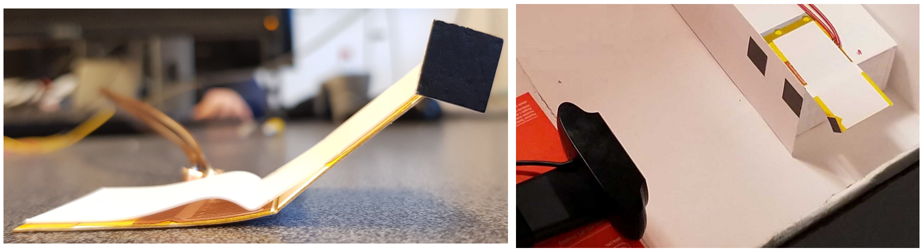

(a) Single hinge prototype

(b) Camera setup

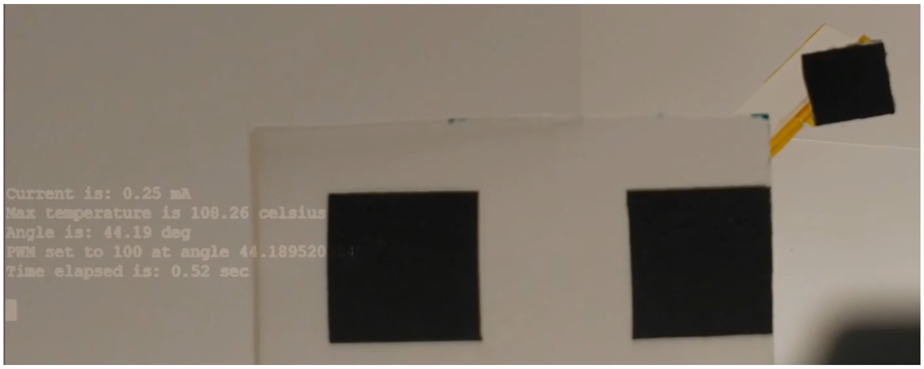

```
Current is: 0.25 mA
Max temperature is 108.26 celsius
Angle is: 44.19 deg
PWM set to 100 at angle 44.189520
Time elapsed is: 0.52 sec
```

(c) Controlled bending process

Figure 42: Single Hinge design

The open-loop test case 1 is seen in figure 43 where the outcome of the bending angle was different each time, but the measured temperature was quite accurate. Turning off the current at a fixed time without previous observations will give angles with a high variance, which argues that the open-loop system is insufficient, hence there will be difficulties modelling the state-space model.

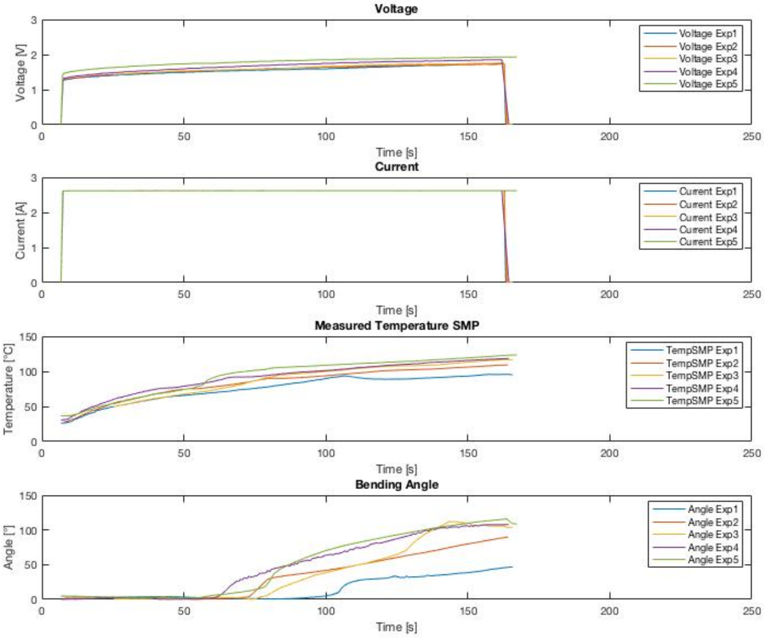

Figure 43: Fixed time, turned off at 2 min and 36 seconds

The closed-loop test case 2 and test case 3 is shown in figure 44 and figure 45. Here the interesting investigation is what the final angle was when the current was cut off at a specific angle. The figures shows that a majority of the experiments ended up in a final angle close to the desired angle. Due to the result of test case 1, the modelling was based on one specific desired angle experiment. What can also be seen in figure 44 and figure 45 is that the prototypes were heated up to a certain threshold temperature before they started bending, thereafter they will continue bending and when the current was cut off, the temperature decreased and the prototypes eventually stopped bending. This whole process was not linear, therefore the modelling for one specific desired angle was divided into two parts to be able to model it linearly. One part when the SMP is bending and heated when the current is on and the other part when current is cut off and the SMP is cooled down and settling to a final angle. Lastly there are two interesting final bending angles, 45° and 90°. Therefore the state-space modelling was conducted based on two specific desired angle experiments, where each of the experiment gave two models, one for heating and one for cooling of the SMP. Hence, there were in total four state-space models presented. The two specific desired angle experiments were arbitrary chosen to experiment 4 of test case 2 and experiment 3 of test case 3.

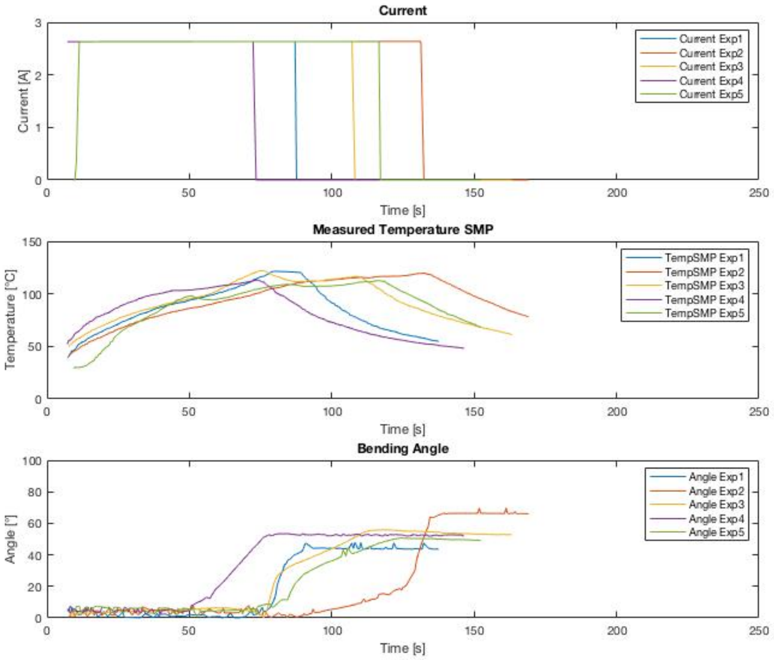

Figure 44: Desired angles around 45°

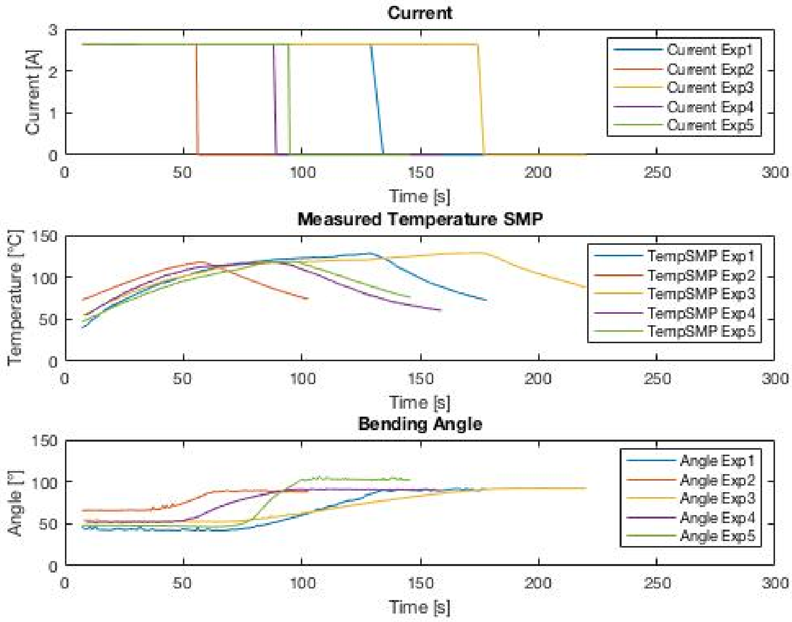

Figure 45: Desired angles around 90°

The result of the closed-loop test case 4 is shown in figure 46. In this test case it can be seen that the bending angle tended to go backwards in the beginning of the bending, which resulted in negative angular velocity. This phenomena was also observed in Felton's article [5]. Felton's observations showed that it could bend slightly -5° before the actual folding, which was believed to happen due to the SMP expanding before it actually shrinks. However this part of the bending process is not of interest for this test case and as the conclusion made from test case 1 the bending process varies a lot. The useful data is therefore the angular velocity and angle at the time when the current is cut off and when the angle has settled.

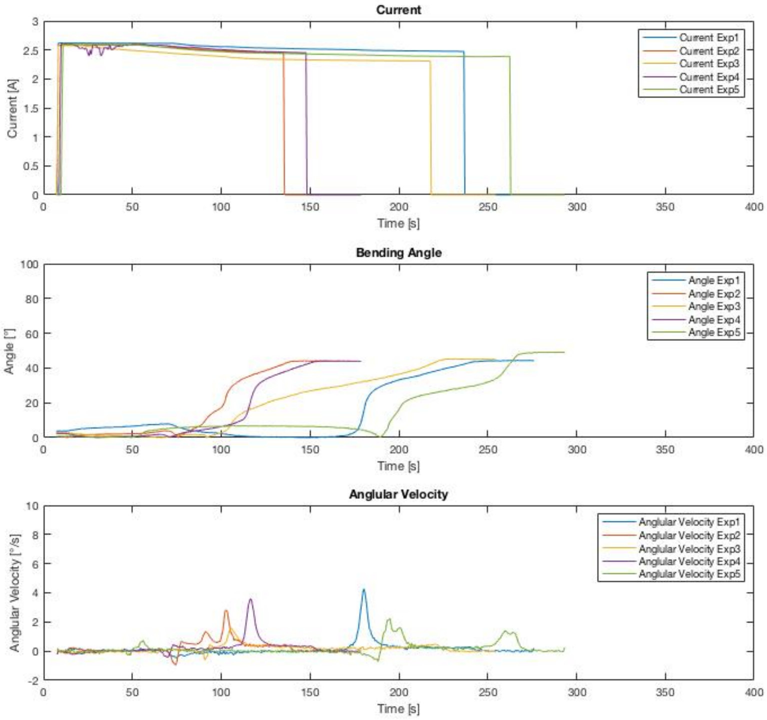

Figure 46: Current turned off when angle reached 42°

Double Hinge Design

The tests of the double hinge design proved to be all successful. In figure 48a, one can see that the materials were able to support an additional hinge even as that outermost hinge heated up and started to bend. In figure 47c, the desired result of the concept design is achieved, with one 90° hinge followed by a 45° hinge.

(a) Start of bending process

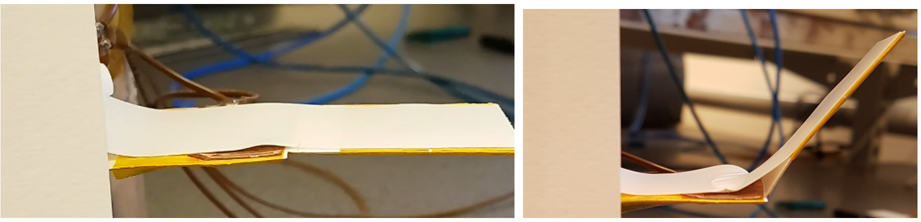

(b) Hinge 1: 90° , Hinge 2: 0°

(c) Hinge 1: 90° , Hinge 2: 45°

Figure 47: Double Hinge design bending to 90° and 45°

In figure 48b, the control system was validated, with successful double angle tracking with the computer vision and switching of the current driver at pre-specified angles. This test also showed that the switched case with first a 45° hinge and later a 90° hinge was possible, demonstrating a high process flexibility.

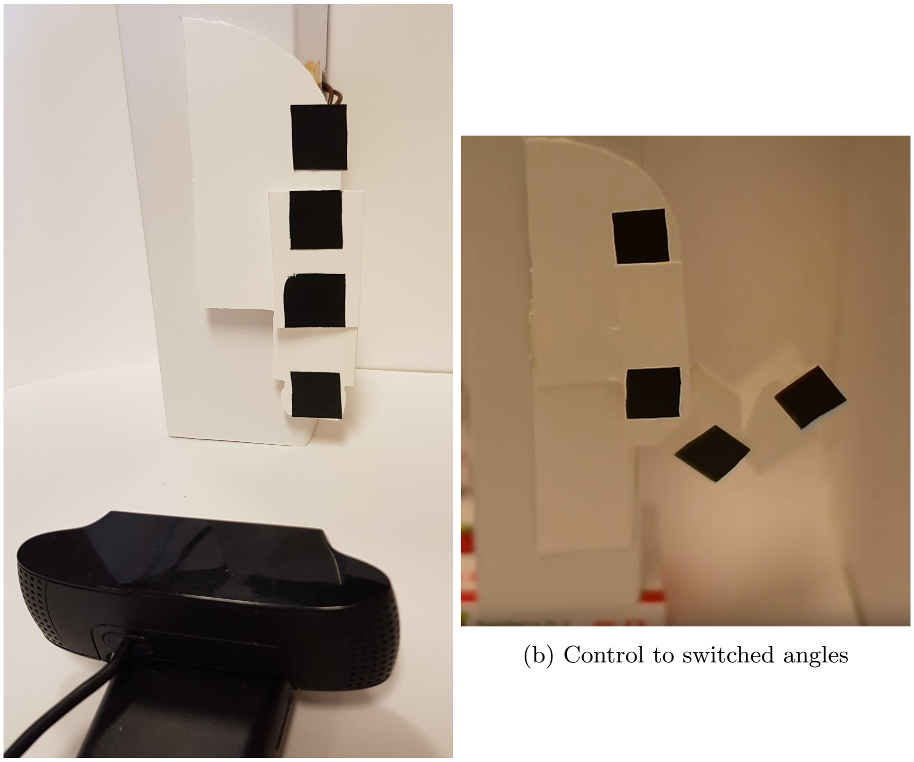

(b) Control to switched angles

(a) Computer vision setup

Figure 48: Double Hinge design computer vision control

6.2 Specifications for SMP

Experiment 4 in test case 2 is shown in figure 49a and figure 49b, where the area to model was interpolated with a sampling time of 0.25s. Figure 49a shows the area when the current is on and the SMP is heated and bending, figure 49b shows the area when the current is cut off and the SMP is cooled down and eventually stops bending.

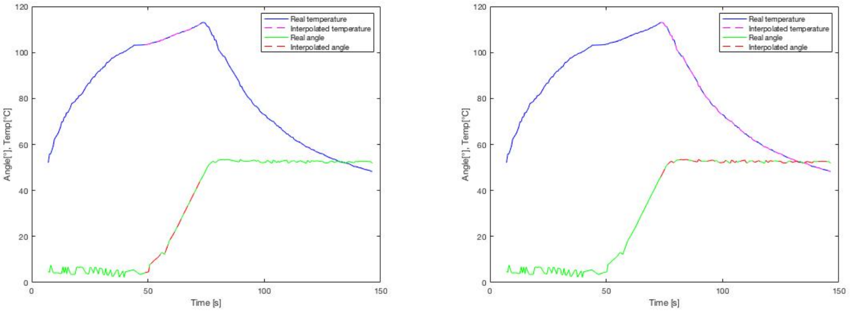

(a) Heated SMP

(b) Cooled SMP

Figure 49: Area of modelling for experiment 4 of test case 2, desired angle 42°

A unit step input with step time at zero is used to evaluate the estimation models. The step response of the three estimation methods to find the state-space models is shown in figure 50a and figure 50b. It is seen in both figures that ”n4sid” is the most suitable and is therefore chosen.

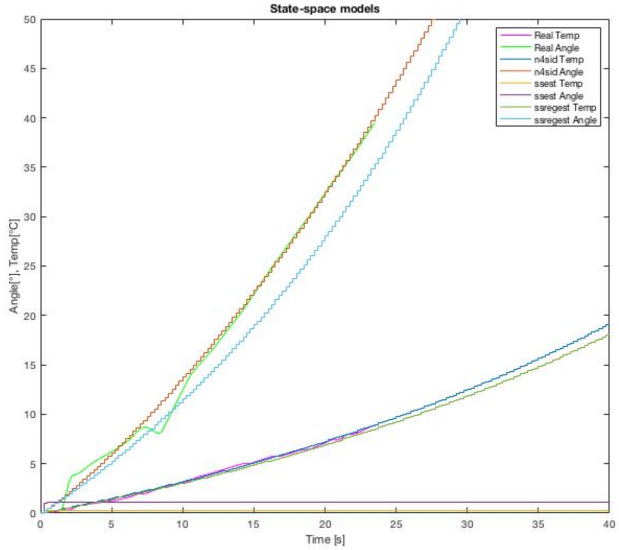

(a) Heated SMP

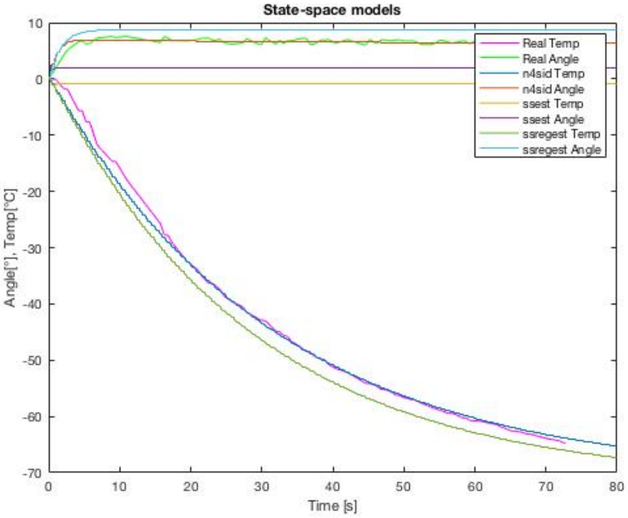

(b) Cooled SMP

Figure 50: Step response of three estimation methods for experiment 4 of test case 2, desired angle 42°

The state-space matrices for the area when the SMP is heated and bending is seen in equation 7 where the initial temperature is 103.33° C and the initial angle is 4.24°. The state-space model for the area when the SMP is cooled down and settling to a final value is seen in equation 8, where the inital temperature is 113.02° C and the initial angle is 45.92°. These matrices describes a state-space model according to equation 1 and equation 2.

$$A = \begin{bmatrix} 1.007 & 0.006017 \\ -0.01222 & 0.9034 \end{bmatrix}, B = \begin{bmatrix} 0.002614 \\ 0.009266 \end{bmatrix}, C = \begin{bmatrix} 22.21 & 1.78 \\ 101 & -2.653 \end{bmatrix} \tag{7}$$

$$A = \begin{bmatrix} 0.9923 & -0.0009396 \\ 0.05499 & 0.7925 \end{bmatrix}, B = \begin{bmatrix} 0.0009038 \\ -0.216 \end{bmatrix}, C = \begin{bmatrix} -295.6 & 0.8969 \\ -1.446 & -6.811 \end{bmatrix} \tag{8}$$

Similar investigation as for the desired angle at 45° was made with the desired angle at 90°. The modelled area is interpolated, shown in figure 51a and figure 51b.

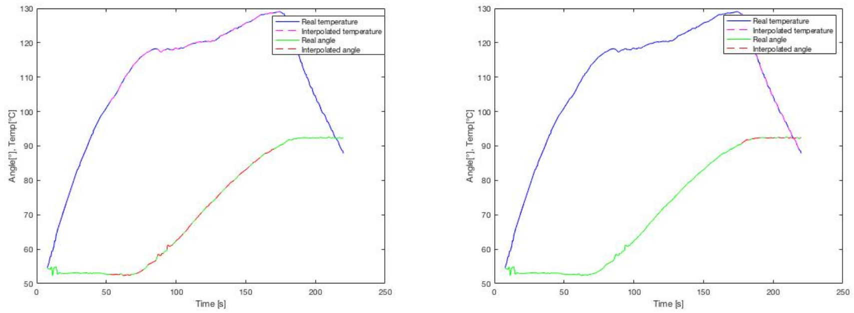

(a) Heated SMP

(b) Cooled SMP

Figure 51: Area of modelling for experiment 3 of test case 3, desired angle 90°

The step response of the three estimation methods is here compared in figure 52a and figure 52b. For these models it is also considered that the subspace method is the most suitable.

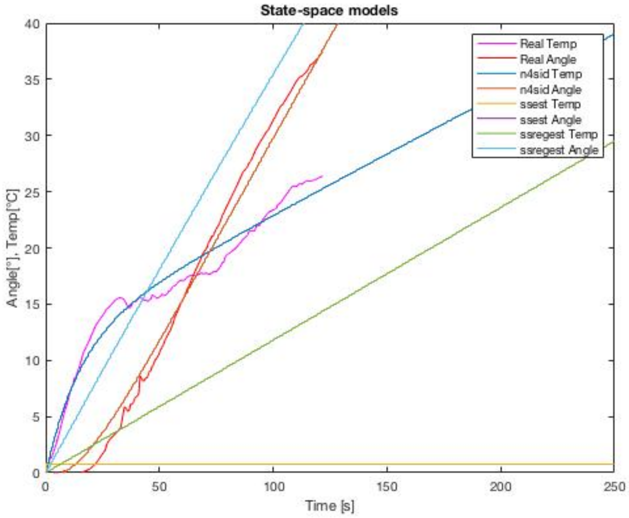

(a) Heated SMP

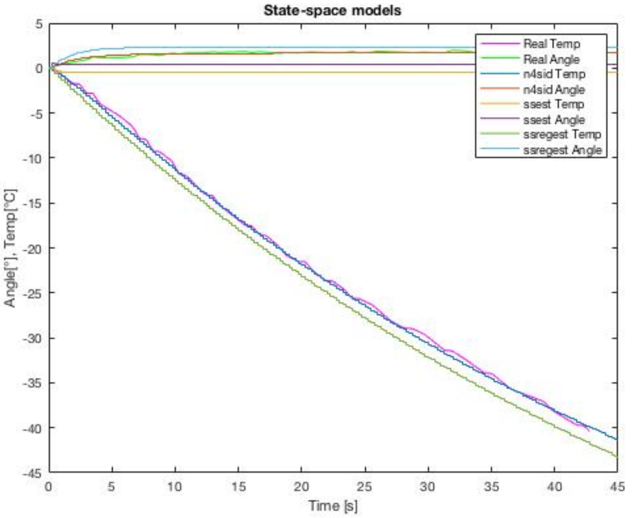

(b) Cooled SMP

Figure 52: Step response of three estimation methods for experiment 3 of test case 3, desired angle 90°

With the same model representing as equation 1 and 2, the state-space matrices for the heated SMP with desired angle at 90° is seen in equation 9 with initial temperature at 102.68° C and initial angle at 52.67° and the state-space matrices for the cooled down SMP is seen in equation 10 with initial temperature at 128.40° C and initial angle at 90.63°.

$$A = \begin{bmatrix} 0.9995 & -0.000494 \\ -0.01392 & 0.9836 \end{bmatrix}, B = \begin{bmatrix} 0.0004608 \\ 0.004736 \end{bmatrix}, C = \begin{bmatrix} 122.3 & 35.65 \\ 274.8 & -31.83 \end{bmatrix} \tag{9}$$

$$A = \begin{bmatrix} 0.9959 & -0.0005395 \\ 0.05289 & 0.8859 \end{bmatrix}, B = \begin{bmatrix} 0.002037 \\ -0.07977 \end{bmatrix}, C = \begin{bmatrix} -139.4 & -0.8864 \\ 1.939 & -2.137 \end{bmatrix} \tag{10}$$

The prediction model was achieved by test case 4 where the final angle, final angular velocity and angular velocity (when current was cut off) was obtained by reading from figure 46. The prediction model is therefore valid for angles around 45°. The angular velocity when the current was cut off and the angle change (from when current was cut off to final angle is settled) was plotted to find a polynomial to fit the points. It is seen in figure 53, that there are four points that can fit a first degree polynomial, if experiment 2 is neglected, which results in the linear equation 11.

$$y(x) = 4.6095x + 0.7624 \tag{11}$$

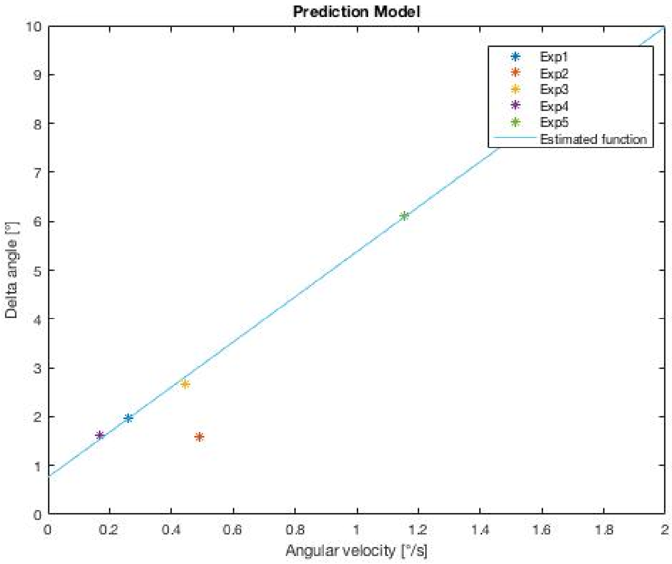

Figure 53: Prediction model for angles around 45°

The temperature of the copper was obtained by test case 1, equation 4 and equation 5. It is seen in figure 54 that the temperature of the copper is higher than the temperature of the SMP, besides that the behaviour is similar. This shows the heating dynamics of the system, where the heat conductivity between these materials can be seen as low with a constant deviation. As the temperature of the copper evens out, so does the SMP temperature, but at a lower value. This clearly requires a heating element at a much higher temperature than the desired temperature of the SMP, which is a learning that has to be taken into account when selecting system components. Luckily, the system for the project was built with a sufficient margin to support this increased temperature of the heating circuit.

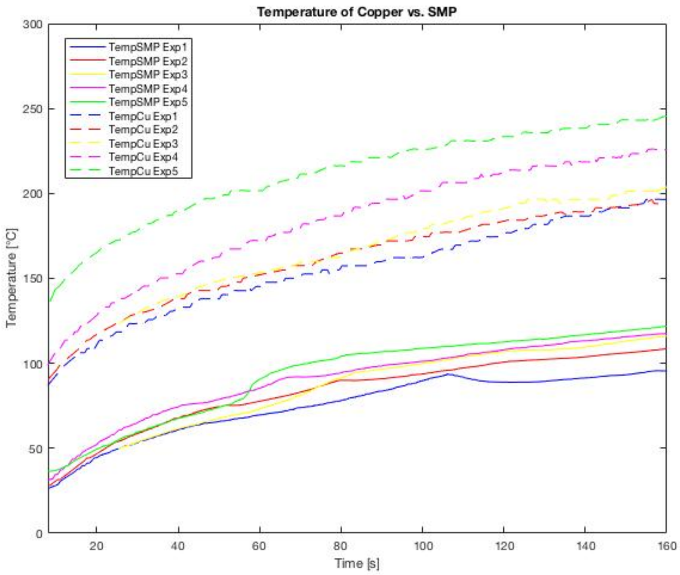

Figure 54: Temperature of the copper circuit and the SMP

6.3 Controllability & Precision

6.3.1 Simulation result

The MPC controller was firstly tested in simulation. Two state-space models were used to simulate the heating behavior and cooling behavior. The heating model is derived from one experiment when the SMP started to bend at 4.24° and 103.33° C. The cooling model is derived from the same SMP sample, where the current was cut off at 45.92° and 113.02° C.

The sampling time Ts was 0.25s, the time horizon of MPC controller was N = 40, which means the controller predicts next 10 seconds each time.

At time 0, Initial state $x_0 = [105, 4]$ (temperature and angle). According to the prediction, the current should be cut off after 34 sampling time, which is at 8.5 seconds. The final angle will be 44.84 degree.

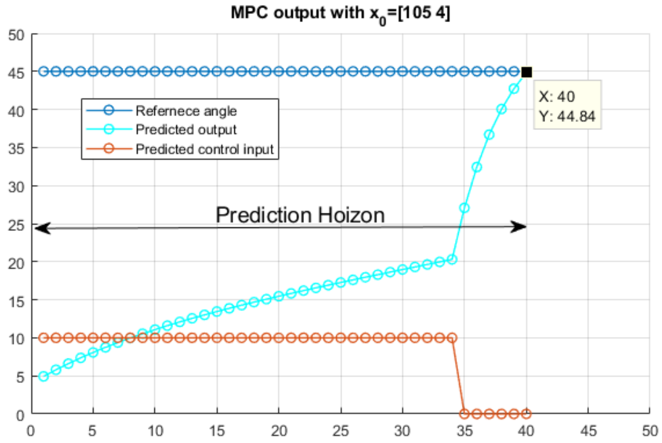

Figure 55: MPC output

From the result, when the current was turned off, the angular velocity increased abnormally, which also conflicted the actual experimental observation.

The reason for that is the actual model in nonlinear. The transfer function for cooling model is obtained from the experiment where the current was cut off at the bending angle of 42° and the temperature of 113° C. It has a very short time constant and limited DC-gain, which causes the angle to rise up to a fixed angle in a few sampling times regardless the initial state. When the state is not around the linearization point, the transfer function will not be able to accurately describe the model behavior.

In the simulation, the temperature and angle at cutoff moment was 106° C and 27°. The cooling model is not practical for this situation.

6.3.2 Practical Experiment Result

The prediction model was implemented in the code and tested, where the current was cut off when the predicted angle reached a value equal or larger then 45°. The desired angle at 45° was not always achieved but the final angle was well predicted. The real angles follows the predicted model, as can be seen in figure 56.

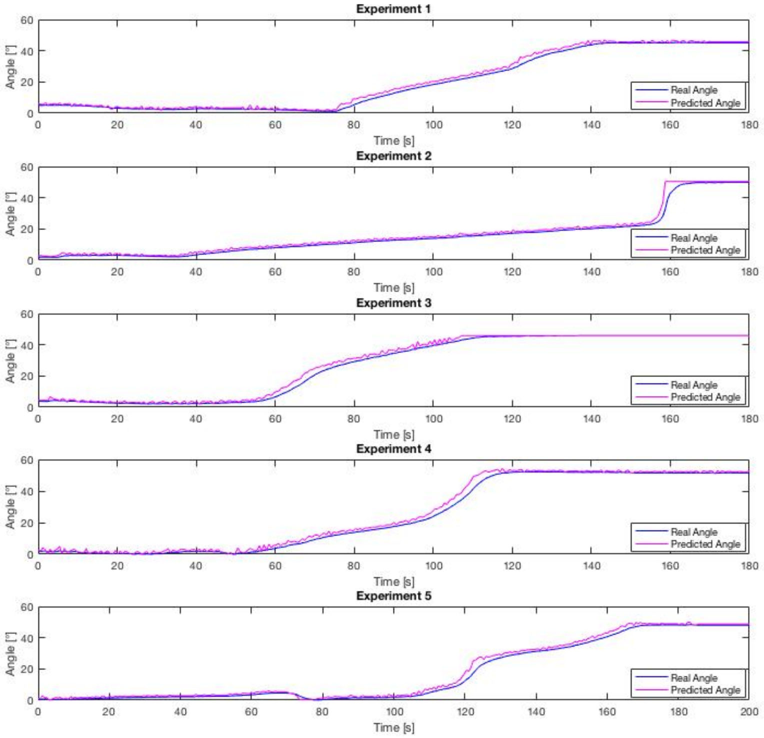

Figure 56: Implemented prediction model for angles around 45°

6.4 Open-Loop vs Closed-Loop

The angles at the turn off time in the open-loop test case 1 is seen in table 8. It can be seen that the variance of the angles is high although the exact same experiment was done five times. Therefore it can be assumed that the system is unable to be controlled by only considering the time for turning off the current.

	Exp 1	Exp 2	Exp 3	Exp 4	Exp 5
Angle[°]	45.83	89.39	103.48	107.92	108.61

Table 8: Open loop

By observing the current angle and turning off the current when 42° was reached as in test case 4, the system is controlled closed-loop. In table 9, "Stop Angle" refers to the current angle when current was turned off. It can be seen that the final angle is close to the desired angle 45° with the lowest value at 43.9° and the highest value at 49°. It is also notable that the lowest value has the lowest velocity when current was turned off. The same goes for the experiment with the highest final angle, where the velocity is the highest.

	Exp 1	Exp 2	Exp 3	Exp 4	Exp 5
Stop Angle[°]	42.24	42.40	42.32	42.27	42.88
Final Angle[°]	44.2	44	45	43.9	49
Stop ω[°/s]	0.26	0.49	0.44	0.17	1.16

Table 9: Closed loop without prediction model

By adding observations of the angular velocity, the predicted model equation 11 could be achieved and implemented as closed loop control, which gave the performance in figure 56. More specific information is shown in table 10, where it can be seen that when the predicted angle is around 45°, the final angle is close to 45°, with the lowest value at 45.06° and highest value of 48.02°. Experiment 2 and experiment 4 predicted a value larger than 45° , but it should be noted that the final angle is close to the predicted angle. The stop angles for experiment 2 and experiment 4 are lower and the angular velocities are larger compared to the rest of the experiments, which means that the prediction model is working, knowing that when the velocity is high the current should be cut off earlier.

	Exp 1	Exp 2	Exp 3	Exp 4	Exp 5
Stop Angle[°]	42.98	39.16	43.37	41.53	43.15
Final Angle[°]	45.06	49.94	45.93	51.50	48.02
Stop ω[°/s]	0.57	6.05	0.47	2.46	0.88
Predicted Angle[°]	45.34	50.42	45.83	49.16	45.82

Table 10: Closed loop with prediction model

6.5 Bucky Gel Manufacturing

This section covers the fabrication process as performed during this project. It is based on the production process mentioned in the Methods & Implementation section, but as the replicability of the article was low, some alterations needed to be done as unsuccessful samples were created.

The chemicals were mixed together and put into ultrasonic bath. The casting process was delayed as the PVDF did not dissolve in the solvent (PC and MP) until a day later. DMAC, which was used as the solvent in the paper of Mukai [10], was fortunately found in the lab and it proved successful to be used as a solvent for PVDF. The solution was then remade and put in an ultrasonic bath for 3 hours.

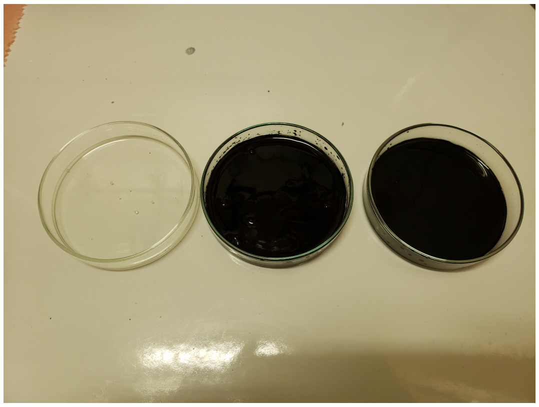

Figure 57: First Bucky Gel results

In figure 57, one can see the first results of the electrode solution and the electrolyte solution. The next step is the casting process, which will be done after the solvent has been evaporated in the oven. Although, as can be seen in figure 58, the electrolyte layer looks fine but the electrode layer has scattered into small fractions.

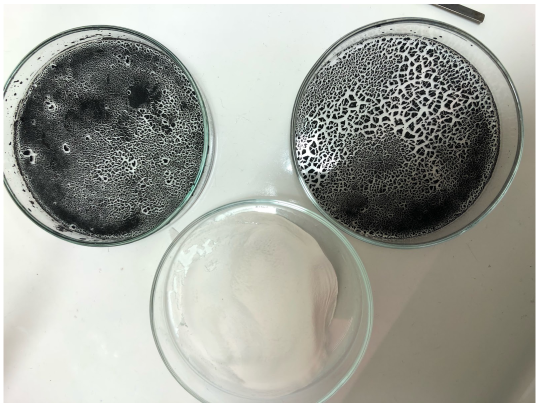

Figure 58: Bucky Gel evaporation results

Another problem is that the electrode layer sticks to the petridish and it's hard to take out. The reason might be that the petridish is too big so the solution does not have enough thickness to become a film. To solve this, the electrode material was recycled and dissolved again. A new smaller mould has been made with silicon film, which the solution will be cast in next.

After contact with the authors of the article that the process follows, advice were given that an aluminum film could be used to cover the base of the casting mould. Additionally, the layer should not be excessively dry.

A new mould was 3D-printed and covered with this aluminum film. Both electrode and electrolyte layer was re-dissolved and cast into the new mould.

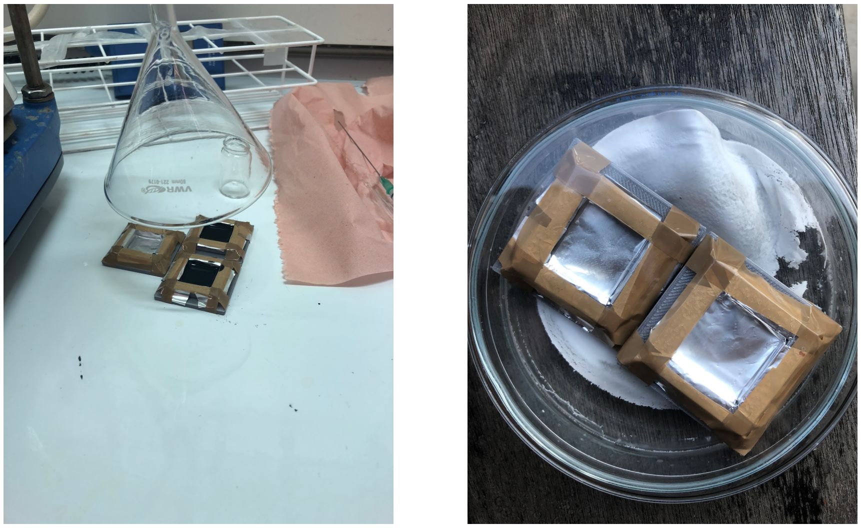

(a) Evaporation set up (b) Electrolyte layer

Figure 59: Bucky Gel fabrication tests with new moulds

This test was more successful, with a solid electrode film after the solution casting process, as can be seen in figure 60.

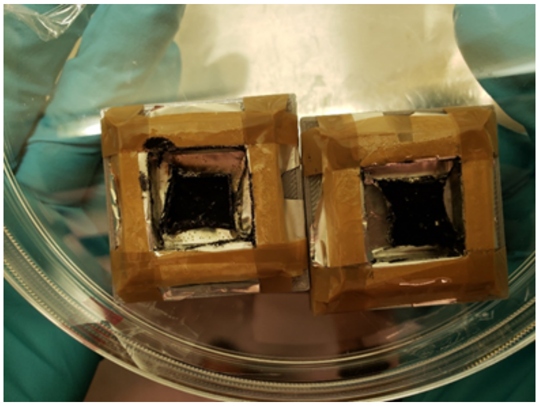

Figure 60: The electrode layer after solution casting

The next step is to hot press the electrode film and electrolyte film together. For this, a special hot press machine is used, shown in figure 61.

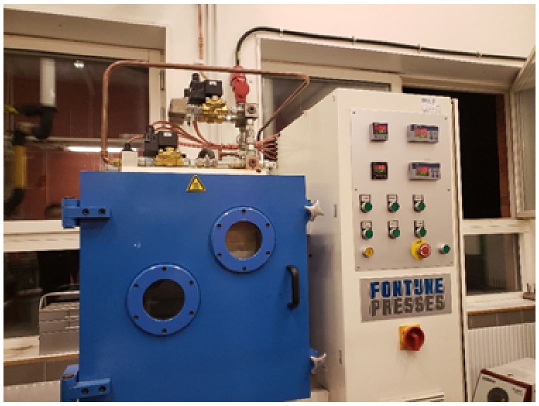

Figure 61: Hot press equipment

In figure 62 one can see the effect of the hot press step, with pictures of both before and after. The settings for the hot press machine is shown in figure 63

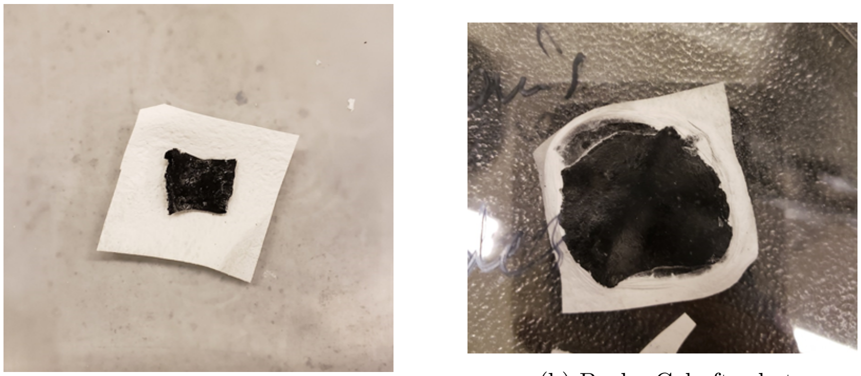

(a) Bucky Gel before hot press

(b) Bucky Gel after hot press

Figure 62: Bucky Gel hot press joining of actuator layers

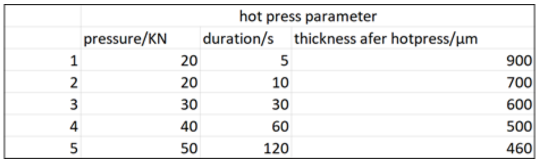

	hot press parameter		
	pressure/KN	duration/s	thickness afer hotpress/µm
1	20	5	900
2	20	10	700
3	30	30	600
4	40	60	500
5	50	120	460

Figure 63: Hot press settings

The first iteration of the manufacturing process had now been completed, with a complete Bucky Gel actuator as a result. It was cut into strips and tested with different voltage levels. This can be seen in figure 64.

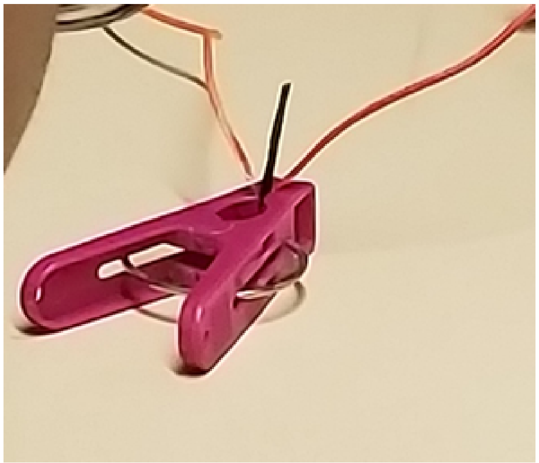

Figure 64: Bucky Gel bending test

However, no bending was achieved at any voltage level. The conductivity between the electrode layers was tested in order to make sure that the design had not been short circuited, but it was found to be non-conductive and therefore should be functioning.

The reason we guess as follows. The CNT layer is too thick and the electrolyte layer is too thin to provide enough ions to bend the Bucky Gel. The ions will transfer to the cathode and anode layers when applying the voltage, which cause the Bucky Gel bend. If there is not enough ions to make the swelling of the cathode layer and shrinkage of the anode layer, then the Bucky Gel will not bend.

The second reason may be that too much hot pressing force makes the gel too dense to deform. The thickness of electrode layer is thicker than the electrolyte layer after solution casting process which cause much hot press pressure to get the ideal thickness of three layers. If the final electrode layer is too dense, then the Bucky Gel will not bend.

The manufacturing process was initiated again, this time with square moulds. However, in the attempt to make the design less thick after the non-bending prototype, the new solution came out too thin. This can be seen in figure 65, where the carbon nanotube layer is scattered and the electrolyte layer invisible.

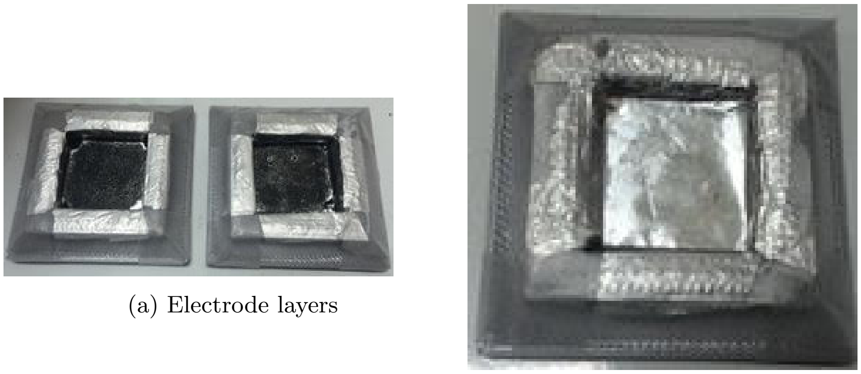

(a) Electrode layers

(b) Electrolyte layer

Figure 65: Bucky Gel hot press joining of actuator layers

The process was done once again, with new moulds and thicker aluminum foil, which can be seen in figure 66. This enables a higher volume of the solutions at one time.

Figure 66: Bucky Gel casting

For this test, the hot press wasn't used, since the pressure is too high, making the final actuator too stiff. Instead, the layers were gently pressed together by a bottle of water. Sadly, the the electrode layer was once again scattered as seen in figure 67. This time however, it was made more like a film, which can be seen in figure 68. The electrolyte layer seems more stable, and came out well this time as well.

Figure 67: Evaporation results

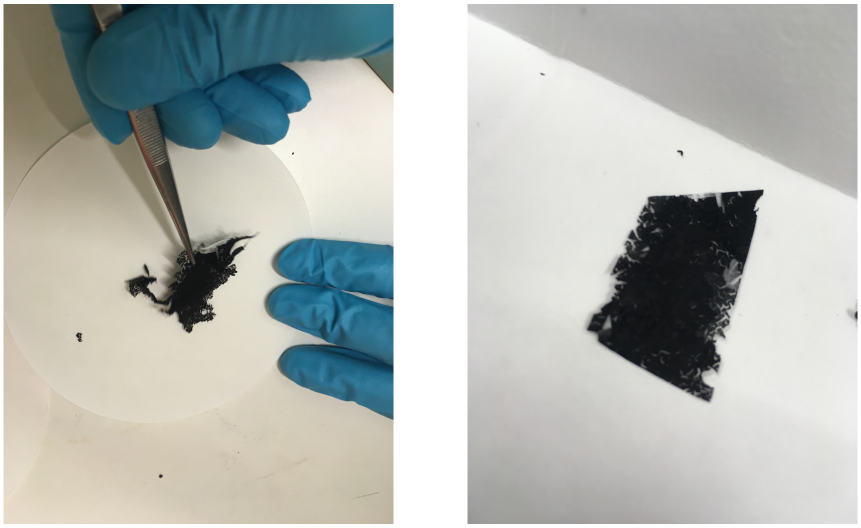

(a) Electrode film

(b) Electrode film

Figure 68: Bucky Gel casting

After the more gentle joining of the layers, that actuator was able to bend for the first time. This was a big step for the project, showing the potential of the material. When switching the positive and negative electrode and it bent in the other direction, exactly as desired. During the test, simple tape was used to hold the design in place. However, this tape burned during one attempts, and when it was replaced, the Bucky Gel actuator burnt instead. The burning probably occurred due to the fast voltage increase to 6V, when the actuator did not respond to the expected 3V.

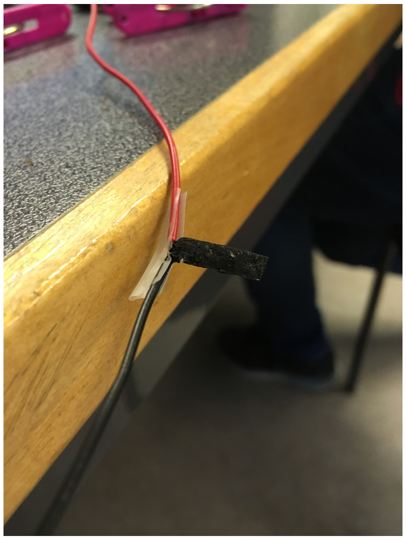

Figure 69: Bucky Gel bending for the first time

After the first successes with the material, more Bucky Gel was made, as shown in figure 70. This time, both the old CNT and the new CNT were used, to recycle the materials. This is shown in figure 70.

(a) Electrode layers

(b) Electrolyte layers

Figure 70: Bucky Gel casting

The new production of electrode layer scattered again, probably due to that the mould was too big. One could also see some liquid on the petridish under the tin foil. Either the tin foil was accidentally destroyed during the preparation, or that the DMAC solvent dissolved it.

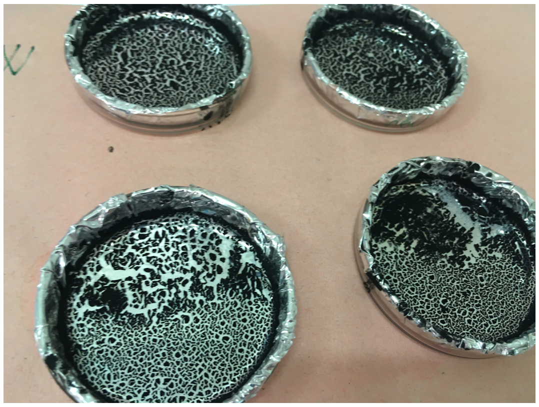

Figure 71: Scattered Bucky Gel electrodes

The last try for remaking the Bucky Gel layers were done with small moulds, as seen in figure 72. The result was scattered again, so the problem is not the size of the module but something else. Contact was yet again established with the previous researchers, who replied saying that their stated carbon nanotube weight percentage of 43% in the electrode solution may be too small.

(a) Before evaporation

(b) After evaporation

Figure 72: Last real Bucky Gel fabrication test

Focus shifted towards making demonstration samples for the end of the project. These were thicker than before, and was not meant to be actuated. The result can be seen in figure 73, where one non-scattered electrode layer was produced.

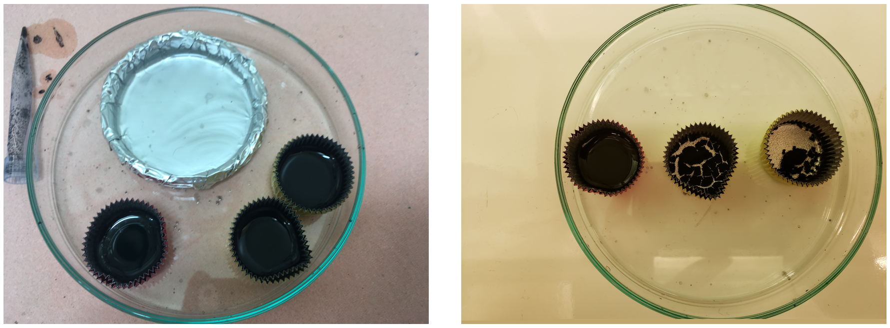

(a) Before evaporation (b) After evaporation

Figure 73: Bucky Gel demo fabrication

The successful fabrication was hot-pressed to actuators shown in figure 74 to the left. To the right, a more sophisticated holding equipment is shown, as the previous tape construction wasn't suitable.

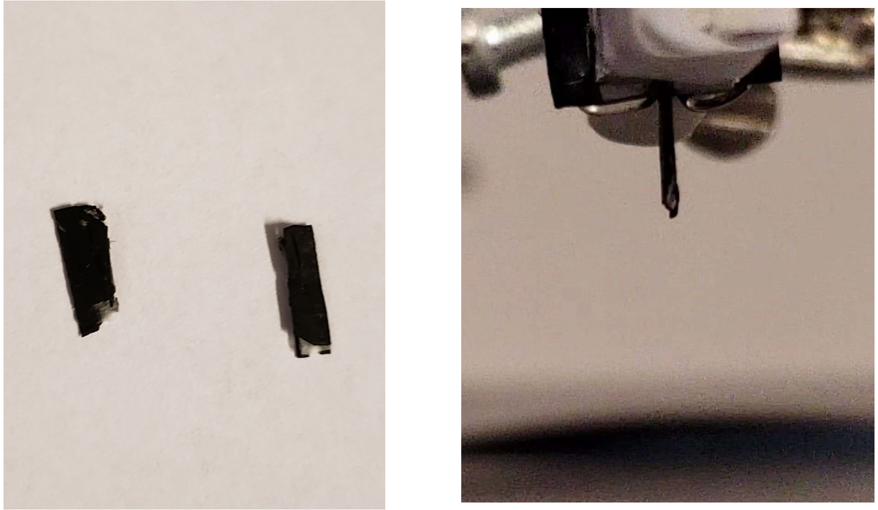

(a) Bucky Gel strips (b) Testing rig

Figure 74: Final Bucky Gel setup

7 Discussion & Conclusion

This section covers the discussion of the project results, as well as provides conclusions to these topics.

7.1 Shape Memory Polymer

As can be seen from the results, the SMP prototypes behave differently each time, despite being produced and stimulated the same way. One of the reasons behind this could be the uncontrolled pressure of placement on the tape or the accuracy of placement of the heating circuit and SMP layer. The heating circuit and SMP might not always be placed on the same width for all the layers, which causes differences on prototyping. It should be noted that the prototyping variance has been reduced as much as possible during the actual manufacturing of the layers, but it can't be fully eliminated due to the human factor when assembling each layer for the prototype. The intended goal of automating this process with an advanced multi-material printer would however be able to do exactly this, and as such it is but a passing problem. One more probable reason behind this is the unevenness of the commercial shrink film used, as it never has been produced for this purpose. The material can therefore not be assumed to be homogeneous, which is also partly why it was investigated.

To enable a more complex control of the process, where modelling of the system is required, there is a need for a more homogeneous material. Then it would be possible to find a state-space model of the system, which can be used as a plant for the control design. Due to different outcome of each test in this project, it is not possible to find a general model for the SMPs behaviour. From test case 2 and test case 3, one result from each was used to obtain a theoretical state-space model for those specific cases. Even though these models are insufficient in explaining the actual system behavior, it shows the method for a more general case with a homogeneous and predictable material. This could then be used to find a state-space model of the whole system. The complex model for this report was therefore only theoretically obtained, but shows a viable strategy for a case where this is possible.

For the less complex closed-loop control with the predicted model, it is seen in figure 53 that the prediction model is only based on 4 experiments, where 3 of them have a lower angular velocity when the current is turned off. The very last experiment 5 with higher angular velocity could be seen to follow the linear equation too. The two inaccurate results seen in table 10 had velocities of 2.46°/s and 6.05°/s, which was much higher than the highest velocity (1.16°/s) of the experiments in table 9 upon which the prediction model was built. The variance of the final angles with lower velocities in the closed-loop control with prediction model was lower (45.06° to 48.02°) in comparison to the variance of the final angles in the closed-loop control without prediction model (43.9° to 49°). In conclusion, the result of the closed-loop control with prediction model was accurate in achieving the desired angle of 45° when the velocity was lower. This should noted to be achieved despite the prototype variance, which shows as predicted that cheaper materials with high variance can successfully be controlled through a closed-loop design.

However, in the case of a higher angular velocity at current cutoff, the control can still be improved. In all experiments, the current was turned off when the predicted angle was equal to or larger than 45°. For experiment 2 in table 10, the predicted angle was 50.42° and from the gathered data the previous sample predicted an angle of 36.78° which is a lot below 45°. It can also be seen that the angular velocity for this experiment was significantly high, and it is here evident that the current computational process is too slow to handle this fast dynamic. In other words, a higher angular velocity requires a higher sampling frequency, or inversely a lower sample time. As the velocity is higher in the angular range around 45° than at 90°, this restraint is more evident in these cases.

From experiment 4 in table 10, the predicted angle was 49.16° when the current was turned off, but the previous sample predicted an angle of 46.43° when the current was on. Here the problem is not the sample time, because the previous predicted angle was close to 45°. The real cause could be due to the computational delay. There is always a computational delay from the time when the predicted angle is larger or equal to 45° is detected to the time when the current is actually cut off. However, for lower velocities as in experiment 1, 3 and 5, it did not affect the system significantly, as the angular velocity was low. For experiment 4 with higher velocity, the predicted angle changed due to the delay time to actually turn off the current.

Even though the prediction model presented in this project did not always achieve the desired final angle, it was verified that the final angle was predicted accurately. Research in the field is still in an early stage, and applicational readiness is distant. In conclusion, the sample time of 0.6s used for this project gave accurate results for cases with lower velocity, but for higher velocities the computational time and sample time must be faster.

7.2 Bucky Gel

For the Bucky Gel actuator, nine experiments were made and only one of them was successfully bent. The electrolyte layer was easy to make but the electrode layer was persistently difficult to produce. For the successful test, a large bending angle of close to 90 degrees was achieved. When switching the positive and negative electrode, it bent in the other direction, exactly as desired. The test voltage was not controlled properly and had to be increased from the expected 3V to 6V for the bending to happen, which also caused more heat generation than expected. The mounting of the Bucky Gel actuator was not designed for this, which resulted in it burning. The following test, the successful Bucky Gel actuator also burned due to this.

Since the limitation of time and experience in this area, it was difficult to make the Bucky Gel successful in each try by just following the manufacture process described in previous articles. Even with contact with the researchers of one the articles, it was hard to follow their procedure, and evidently some critical details of the process is still not known.

The mould size was also a big problem during the solution casting process. A big mould would cause the electrode layer to scatter, while a small mould would make the film too thick to press. That the parameters of some steps, such as the temperature during the drying process or the pressure of hot press, was not controlled properly may also be a reason for the low successful rate of the fabrication process.

During the test process of Bucky Gel, it was difficult to apply the both voltage polarities to such a small and thin strip. The lack of a perfect experimental environment made it difficult to observe and catch the bending of the Bucky Gel. A similar setup to the one for the SMP, with a PCB for voltage control and computer vision for angle detection, would have been the next step should the Bucky Gel be successfully manufactured again.

8 Future Work

This section focuses on what needs to be targeted next by research in the field.

8.1 Shape Memory Polymer

One of the main issues with the SMP was that it did not behave uniformly for each experiment, which probably was the effect of both a human assembly process but more likely an inhomogeneous material. Future research could target the impact of this, and test the homogeneousness by using an advanced oven that spreads the heat evenly, to observe if all the SMP pieces shrinks the same. A more homogeneous material could then also be produced, but it is believed to make the process more expensive. Some of the benefits of the SMP is that it's cheap and easily available, and there is a risk to jeopardize this through this refinement. One could therefore examine the cost-effectiveness of those materials versus the increased controllability. To reduce the error source of the manufacturing process, future work could look into the automation and optimization of the manufacturing and assembly process of the prototype, for example with an effective additive manufacturing process. In conclusion, if above-mentioned improvements could be applied, the outcome would be more predictable and the state-space model could be obtained easily by following the method in this project. The state-space model could also be improved by investigating other combinations of states, such as angular velocity and temperature instead of angle and temperature. The results shows that the angular velocity is an big impact of the process, and temperature may well be an underlying factor for this, maybe also dependent on the angle.

Further improvements can still be made by keeping the cheap SMP material suggestion, since its variance can be controlled by the prediction model. The suggestion is to conduct several experiments with different velocities, mostly with high velocities since that is the inaccurate part of the current model. With more gathered experimental data, the prediction model can fit a better model and better predict the behaviour. When implementing the prediction model, the sample time and computational time should be faster, especially when the velocity is high. Investments in controller hardware to realize this may also increase the product cost, but as this is not consumed and as it is flexible to product variations, it should be justified for large-scale production.

Instead of minimizing the sample time and computational time, one could also try to control the heating process to be slower. In that case, the bending process would perhaps also be slower, which means the angular velocity is lower and the current prediction model control would give a more accurate result. This would however cause an increase of cost and complexity of the controller, because temperature modelling shows that a thermal sensor needs to be added to the process.

The modelling in this project is based on mainly two interesting desired angles, but it is believed that the system is so complex that for different desired angles the model would change. Therefore more models with different desired angles need to be generated to get more accurate predictions, thus making it a multiple input model with both angle and angular velocity dependence.

A more practical issue is the PWM heating of the SMP. The quadratic relationship between power and current changes the heating behaviour of the system when using a PWM signal compared to a DC signal. Future researchers are encouraged to further explore the possibilities of using PWM for heating SMP material in a closed-loop system.

8.2 Bucky Gel

Since one Bucky Gel actuator was successfully bent, the next step is to make the manufacturing process more repeatable. For this, details and parameters during the process need to be more thoroughly investigated, suitable as a thesis project in Chemical Engineering. A better experimental environment is also needed to be set for testing the Bucky Gel, which have been proposed to have a similar characteristics to the SMP setup. As this couldn't be sufficiently tested, the Bucky Gel case may require a testing environment with different properties, which would have to be investigated.

References

[1] Binayak Bhandari, Gil-Yong Lee, and Sung-Hoon Ahn. A Review on IPMC Material as Actuators and Sensors: Fabrications, Characteristics and Applications. *Precision Engineering and Manufacturing*, 13:141–163, 2012.

[2] D. W. Muse D. Espalin and E. MacDonald. 3d printing multifunctionality: Structures with electronics, international journal of advanced manufacturing technology, vol. 72, pp. 963-978. 2014.

[3] E.Pei. 4D Printing: Dawn of An Emerging Technology Cycle. *Assembly Automation*, 34(4):310–314, 2014.

[4] Epilog. Laser systems and printed circuit boards. 2018. http://support.epiloglaser.com/article/8205/42816/laser-systems-and-printed-circuit-boards.

[5] Samuel M. Felton, Michael T. Tolley, ByungHyun Shin, Cagdas D. Onal, Erik D. Demaine, Daniela Rus, and Robert J. Wood. Self-folding with shape memory composites. *Soft Matter*, 9(32):7659–7878, 2013.

[6] Q. Ge, C. K. Dunn, H. J. Qi, and M. L. Dunn. Active origami by 4d printing, smart materials and structure, vol. 23, pp. 1-15. 2014.

[7] Yang W. G.and Lu H., Huang W. M., Qi H. J., and Wu X. L. Advanced Shape Memory Technology to Reshape Product Design,Manufacturing and Recycling. *Polymers*, 6 No. 8:2287–2308, 2014.

[8] Breger J.C., Yoon C., Xiao R., Kwag H.R., and Wang M.O. Self-Folding Thermo-Magnetically Responsive Soft Microgrippers. *ACS Applied Materials and Interfaces*, 7 No. 5:3398–3405, 2015.

[9] Norihiro Kamamichi, Toshiharu Maeba, Masaki Yamakita, and Toshiharu Mukai. Printing Fabrication of a Bucky Gel Actuator/Sensor and Its Application to Three-Dimensional Patterned Devices. *Advanced Robotics*, 24:1471–1487, 2010.

[10] Kinji Asaka Ken Mukai. High performance fully plastic actuator based on ionic-liquid-based bucky gel. *Electrochimica Acta*, 53, 2008.

[11] Z. X. Khoo, J. E. M. T. Teoh, C. K. Chua Y. Liu, S. Yang, J. An, K. F. Leong, and W. Y. Yeong. 3D Printing of Smart Materials: A Review on Recent Progress in 4D Printing. *Virtual and Physical Prototyping*, 10(3):103–122, 2015.

[12] Simon J. Leigh, Robert J. Bradley, Christopher P. Purssell, Duncan R. Billson, and David A. Hutchins. A simple, low-cost conductive composite material for 3d printing of electronic sensors, plos one, vol. 7, no. 11, pp. 1-6. 2012.

[13] MATLAB. Estimate state-space models at the command line. [cited 2018-12-01].

[14] MATLAB. n4sid. [cited 2018-12-02].

[15] MATLAB. ssregest. [cited 2018-12-02].

[16] Caputo MP, Berkowitz AE, Armstrong A, Mullner P, and C.Virgil Solomon. 4D Printing of Net Shape Parts Made from Ni-Mn-Ga Magnetic Shape Memory Alloys. *Additive Manufacturing*, 21:579–588, 2018.

[17] Eujin Pei. 4D printing - revolution or fad. *Assembly Automation*, 34(2):123–127, 2014.

[18] S. Kim R. Niiyama, D. Rus. Pouch motors: Printable/inflatable soft actuators for robotics, ieee international conference on robotics and automation (icra), pp. 6332-6337. 2014.

[19] Jonathan Rossiter, Peter Walters, and Boyko Stoimenov. Printing 3D dielectric elastomer actuators for soft robotics. *Proc. of SPIE*, 7287, 2009.

[20] ByungHyun Shin, Samuel M. Felton, Michael T. Tolley, and Robert J. Wood. Self-assembling Sensors for Printable Machines. 2014.

[21] Dong-Gap Shin, Tae-Hyeong Kim, and Dae-Eun Kim. Review of 4D Printing Materials and their Properties. *Precision Engineering and Manufacturing*, 4:349–357, 2017.

[22] Xu Sun, Samuel M. Felton, Ryuma Niiyama, Robert J. Wood, and Sangbae Kim. Self-folding and self-actuating robots: a pneumatic approach, 2015 ieee international conference on robotics and automation (icra), pp. 3160-3165. 2015.

[23] S. Tibbits. 4D Printing: Multi-Material Shape Change. *Architectural Design*, 84(1):116–121, 2014.

[24] Jing-Jun Wu, Li-Mei Huang, Quian Zhao, and Tao Xie. 4D Printing: History and Recent Progress. *Chinese J. Polym. Sci*, 36:563–575, 2018.

[25] DLiu Y., Genzer J., and Dickey M. D. 2D or Not 2D: Shape-Programming Polymer Sheets. *Progress in Polymer Science*, 52:79–106, 2016.

[26] Lee Y., Lee H., Hwang T., Lee J.G., and Cho M. Sequential Folding Using Light-Activated Polystyrene Sheet. *Scientific Reports*, 5 No. 16544:1–100, 2015.

Appendices

A Project Budget

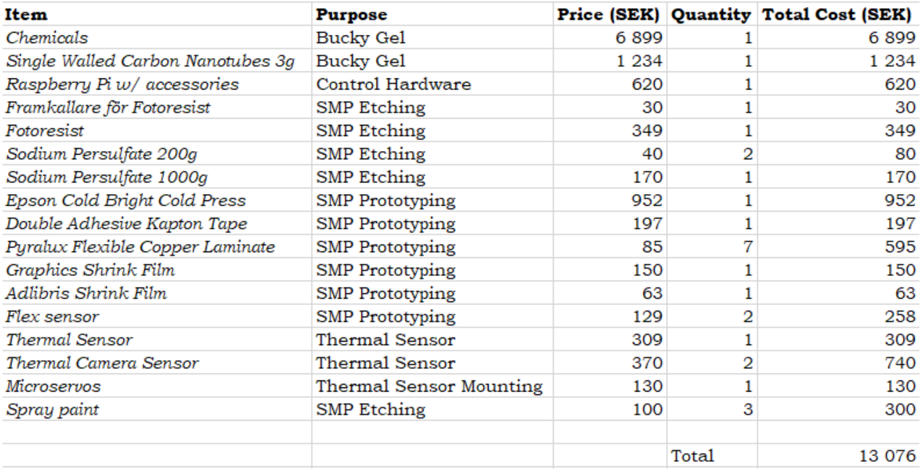

Item	Purpose	Price (SEK)	Quantity	Total Cost (SEK)
Chemicals	Bucky Gel	6 899	1	6 899
Single Walled Carbon Nanotubes 3g	Bucky Gel	1 234	1	1 234
Raspberry Pi w/ accessories	Control Hardware	620	1	620
Framkallare för Fotoresist	SMP Etching	30	1	30
Fotoresist	SMP Etching	349	1	349
Sodium Persulfate 200g	SMP Etching	40	2	80
Sodium Persulfate 1000g	SMP Etching	170	1	170
Epson Cold Bright Cold Press	SMP Prototyping	952	1	952
Double Adhesive Kapton Tape	SMP Prototyping	197	1	197
Pyralux Flexible Copper Laminate	SMP Prototyping	85	7	595
Graphics Shrink Film	SMP Prototyping	150	1	150
Adlibris Shrink Film	SMP Prototyping	63	1	63
Flex sensor	SMP Prototyping	129	2	258
Thermal Sensor	Thermal Sensor	309	1	309
Thermal Camera Sensor	Thermal Sensor	370	2	740
Microservos	Thermal Sensor Mounting	130	1	130
Spray paint	SMP Etching	100	3	300
			Total	13 076

Figure 75: Project Budget